225 (2023) 211704

Contents lists available at ScienceDirect

Geoenergy Science and Engineering

journal homepage: www.sciencedirect.com/journal/geoenergy-science-and-engineering

Sedimentary environment controls on the lacustrine shale lithofacies: A case study from the Nanpu depression, Bohai Bay Basin

Huan Liu [a,b], Xiaoping Liu [a,b,*], Guoyong Liu [c], Guoyong Li [c], Jianwei Wang [c], Yongliang Gao [c], Biao Sun [a,b], Jiakai Hou [a,b], Hanxi Liu [a,b], Xuejiao Sun [d]

[a] State Key Laboratory of Petroleum Resources and Prospecting, China University of Petroleum (Beijing), Beijing, 102249, China
[b] College of Geosciences, China University of Petroleum (Beijing), Beijing, 102249, China
[c] PetroChina Jidong Oilfield Company, Tangshan, 063004, China
[d] No. 5 Oil Production Plant of PetroChina Dagang Oilfield Company, Tianjin, 300280, China

ARTICLE INFO

Keywords:
Lithofacies
Sedimentary environment
Element geochemistry
Lacustrine shales
Nanpu Sag

ABSTRACT

Organic-rich shale of the Paleogene Shahejie Formation in the Nanpu Sag Bohai Bay Basin was analyzed using petrographic and elements analysis. These analyses were used to identify the lithofacies, reconstruct the sedimentary paleoenvironment and their relation. This paper adopted the division scheme and naming method of "Total organic carbon (TOC) + sedimentary structure + mineral composition" to carry out lithofacies identification and division. The petrographical characteristics indicated that there are 15 types of lithofacies. According to the lithologic changes, we divided the study interval from the fourth sub-member of the third member of the Shahejie formation into three parts from the bottom up. The lower part has an evident fluctuation in paleo-climate, salinity, productivity, and redox condition. The middle part has cold and arid climate conditions, the weakest weathering, the highest paleo-productivity, and anoxic conditions. The upper part was deposited under humid and warm climate conditions, strongest weathering, brackish-fresh water, lowest paleo-productivity, and dominant oxic condition. Paleo-productivity and redox conditions are the basic conditions for the enrichment and preservation of organic matter, the paleo-climate and paleo-salinity were the critical factors controlling the mineral composition and laminae development. Under warm and humid climate conditions, the shallow lake mainly develops organic-poor massive felsic shale and siltstone; the semi-deep lake is mainly developed with organic-medium laminated/layered felsic shale; the deep lake mainly develops organic-rich laminated/layered clayey shale and mixed shale. Under dry and cold climate conditions, the shallow lake area mainly develops organic-poor felsic shale, and the semi-deep lake mainly develops organic-rich layered carbonate shale and organic-rich massive mixed shale; the deep lake mainly develops organic-rich laminated/layered clayey shale.

1. Introduction

The shale oil and gas revolution in the United States has achieved great success and changed the world's energy pattern (Qiu and Zou, 2020; Zhao et al., 2020; Zou et al., 2020; Radwan et al., 2022; Zou et al., 2023). Shale oil exploration in China is mainly oriented to continental basins (Liu et al., 2020a, 2020b; Jin et al., 2021). Compared with marine shale, lacustrine shale shows stronger heterogeneity (Jia et al., 2014; Qiu and Zou, 2020; Jin et al., 2021; Wu et al., 2021).

Lithofacies refers to rock types and their assemblages formed in a particular sedimentary environment, resulting from the paleo sedimentary environment (Aplin and Macquaker, 2011; Jiang et al., 2013). Lithofacies reflect the present rock assemblage and the sedimentary environment, which is a further subdivision of sedimentary microfacies (Jiang et al., 2017; Feng, 2019). The description parameters of lithofacies include quantitative and qualitative parameters (Miall and AndrewD, 1990; Lobza, 1999; Ran et al., 2016). The qualitative parameters include color, structure, structure, etc., the quantitative parameters include mineral composition, organic matter content, element composition, etc. At present, mineral composition, sedimentary structure, and organic matter content are widely used (Chen et al., 2016a, 2016b; Liu et al., 2018; Zhang and Li, 2018; Liu et al., 2020a, 2020b). These three parameters determine the reservoir, oil-bearing, mobility, and fracability of shale oil exploration and development to a certain

* Corresponding author. State Key Laboratory of Petroleum Resources and Prospecting, China University of Petroleum (Beijing), Beijing, 102249, China.
E-mail address: liuxiaoping@cup.edu.cn (X. Liu).

https://doi.org/10.1016/j.geoen.2023.211704
Received 30 August 2022; Received in revised form 23 February 2023; Accepted 17 March 2023
Available online 20 March 2023

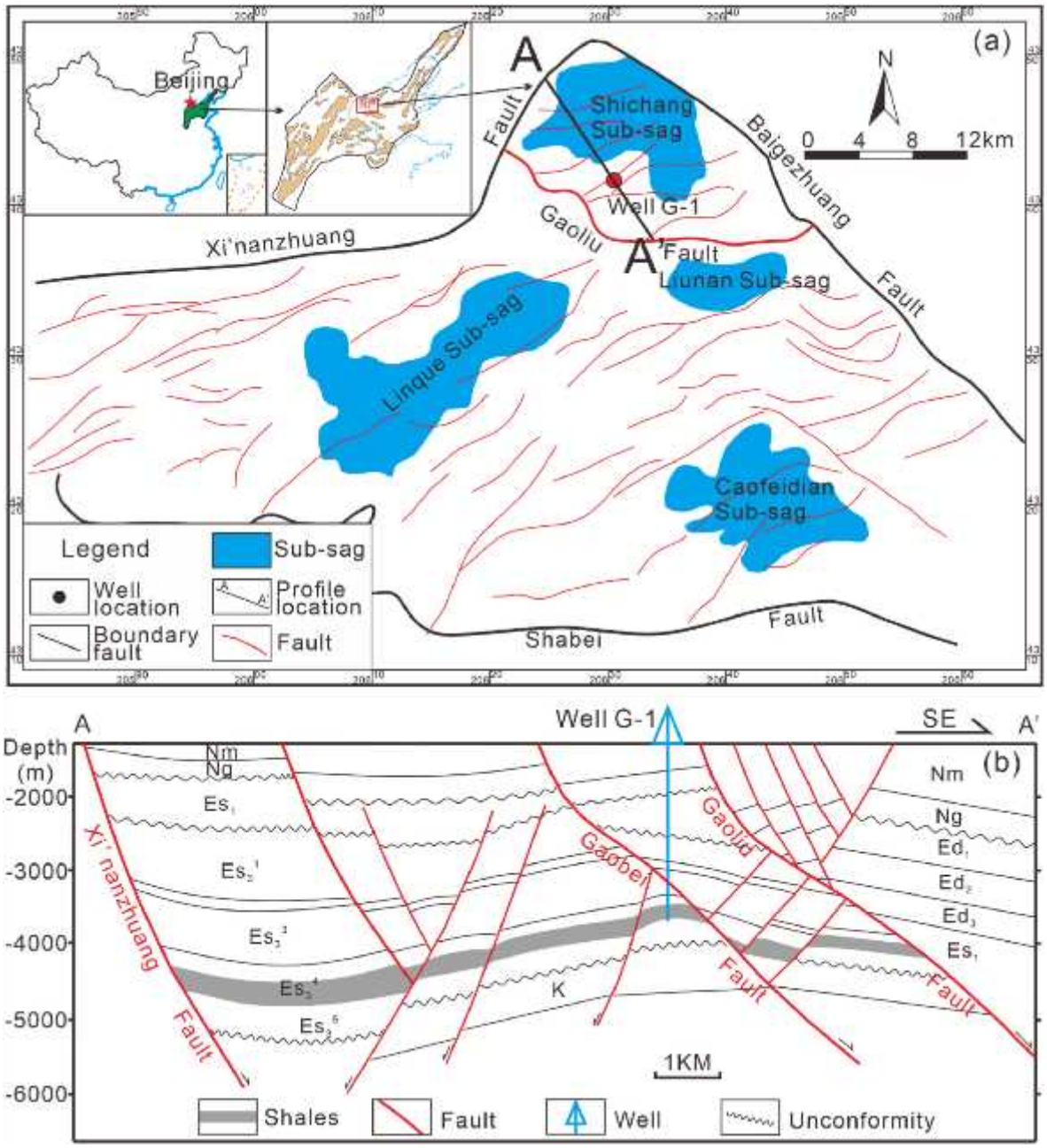

Fig. 1. (a) Geological sketch map of the Nanpu sag showing the location of the sampling well (modified after Li et al., 2019a and Chen et al., 2021). (b) The structural profile of the Gaoliu area, the profile location shown in (a).

extent (Chen et al., 2011; Zhou et al., 2016; Liu et al., 2020a, 2020b; Jin et al., 2021; Hou et al., 2023). As the basic work of shale oil and gas exploration and development, shale lithofacies research has preliminarily formed some consensus on the characterization of lithofacies (Liu et al., 2019; Liu et al., 2020a, 2020b; Liang et al., 2022; Wang et al., 2022; Williams et al., 2022.), but the research on the relationship between lithofacies and sedimentary environment is still weak. The strong heterogeneity of lacustrine basin leads to that there is no ideal sedimentary model that can be well applied to shale oil and gas exploration and development, and much basic research work needs to be further developed. This study attempts to provide some new insights into the relationship between lithofacies and paleoenvironment through element research and lithofacies characterization (Liang et al., 2018; Shi et al., 2020) The faulted lake has a limited water body, poor water circulation, and is sensitive to environmental changes (Picard, 1971; Jiang et al., 2013; Liu et al., 2020a, 2020b). The deposition and distribution of organic shale are often affected by paleoenvironments such as source supply, lake level change, tectonism, and climate (Jin, Z. et al., 2021, Li et al., 2022). In recent years, the Paleogene shale oil resources in Nanpu Sag have shown great exploration potential. The research on the source rocks of Es_3^4 in Nanpu Sag mainly focuses on the organic geochemical characteristics, such as TOC, pyrolysis hydrocarbon, etc. (Chen et al., 2021; Jiang et al., 2020; Li et al., 2019a; Zheng et al., 2007), but little understanding of its paleo sedimentary environment. The formation of source rocks is a complex process involving physical, chemical, and biological interactions (Ma et al., 2022), which is mainly due to the complexity of environmental conditions.

Based on core, thin section, and scanning electron microscope observation of samples, combined with total organic carbon (TOC), systematically analyzes the petrological characteristics of Es_3^4 sub-

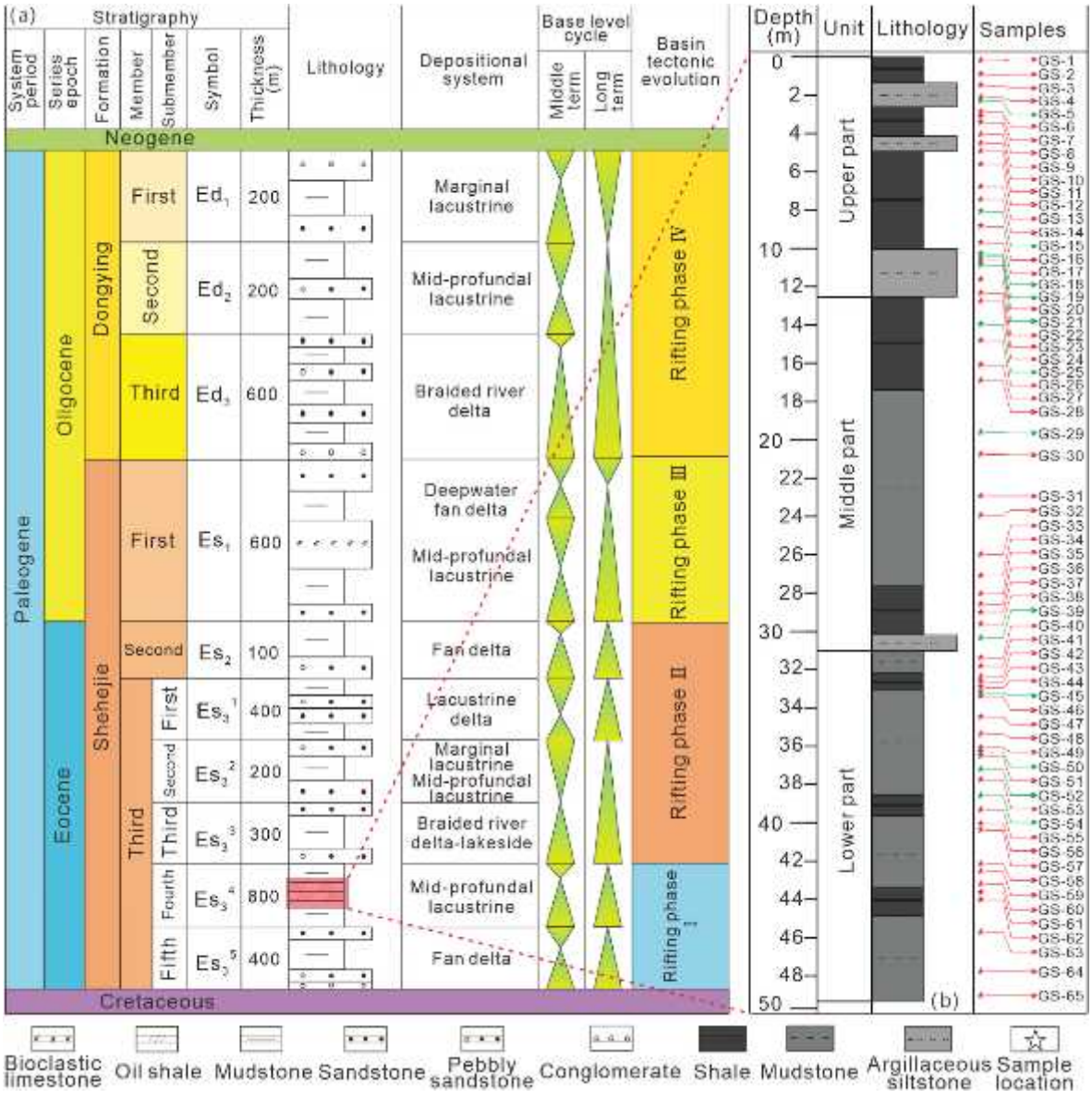

Fig. 2. (a)Stratigraphic column and tectonic evolution of the Paleogene in the Nanpu Sag, Bohai Bay Basin. NE China. (modified after Chen et al., 2021). (b) Lithologic column and sample distribution in the study interval.

member shale in Nanpu Sag, and the lithofacies types and their vertical distribution characteristics are divided according to organic matter abundance, sedimentary structure, and mineral composition. Through the analysis of major and trace elements, the sedimentary paleoenvironment of the Es_3^4 sub-member is reconstructed. Based on lithofacies classification and sedimentary environment analysis, the control effect of sedimentary environment on lithofacies development is discussed.

2. Geological setting

Nanpu Sag is located in the north of Bohai Bay Basin and adjacent to Huanghua sag in the South. It is a fault depression type oil and gas sag developed through Mesozoic and Cenozoic block fault activities, covering an area of about 2.5×10^3 km^2, from north to south, there are four sub-Sags: Shichang Sub-sug, Liunan Sub-sug, Linque Sub-sug, and Caofeidian Sub-sug (Fig. 1a) (Li et al., 2019a). The tectonic evolution of Paleogene strata in Nanpu Sag experienced three episodes of rifting, which controlled different structural patterns and sedimentary filling styles. From bottom to top, the Paleogene successively develop the Es_3 member, Es_1 member, and Dongying Formation. Es_3 member is further divided into five sub-members (Figs. 1b and 2a) (Chen et al., 2021).

The Paleogene Es_3^4 sub-member is a semi-deep to deep lake facies, mainly composed of mudstone, shale, and oil shale, mixed with a small amount of argillaceous siltstone. The Es_3^4 sub-member has a good organic matter type (dominated by types I and II_1), high organic matter abundance, medium maturity (Chen et al., 2021; Li et al., 2019b), and well-developed laminar structure. It is an important stratum for shale oil exploration in Nanpu Sag.

3. Materials and methods

3.1. Samples

The description of the well core from the Es_3^4 sub-member of the Paleogene Shahejie Formation from the G-1 well drilled in the Nanpu Sag was carried out in the core library of Jidong Oilfield. A total of 65 core samples were collected (Fig. 2b) for total organic carbon (TOC), X-ray diffraction (XRD), thin sections, and scanning electron microscope

Table 1
TOC and XRD results of the samples in the Es_3^4 sub-member.

Samples	Unit	TOC	Quartz	Feldspar	Plagioclase	Calcite	Dolomite	Gypsum	Pyrite	Anhydrite	Siderite	Halite	Clay	I/S	Illite	Kaolinite	Chlorite
		(wt.%)	(%)	(%)	(%)	(%)	(%)	(%)	(%)	(%)	(%)	(%)	(%)	(%)	(%)	(%)	(%)
GS-1	Upper part	1.79	23	4	5	18	3	/	1	1	2	/	43	70	20	6	4
GS-2		1.07	21	4	5	20	2	/	1	1	1	/	45	61	26	8	5
GS-3		0.87	25	4	7	18	2	/	/	/	2	/	42	71	21	5	3
GS-4		0.93	22	6	7	14	3	/	1	1	2	/	44	60	27	8	5
GS-5		0.89	38	8	13	3	5	/	/	1	/	/	32	64	24	6	6
GS-6		1.4	38	8	16	3	4	/	/	1	3	/	27	77	12	6	5
GS-7		2.17	32	10	12	5	4	/	/	1	1	/	35	53	27	12	8
GS-8		2	30	5	8	10	/	/	/	1	4	8	34	70	17	9	4
GS-9		2.35	18	2	3	46	9	1	/	/	/	/	21	5	45	35	15
GS-10		1.27	24	9	11	13	2	/	/	1	/	/	40	57	31	7	5
GS-11		1.4	24	5	6	17	2	/	/	1	/	/	45	76	16	5	3
GS-12		2.31	21	8	15	7	2	/	/	1	/	/	46	72	18	5	5
GS-13		2.11	20	5	6	11	2	/	1	1	/	/	54	70	22	5	3
GS-14		2.09	25	4	8	10	2	/	1	1	/	/	49	51	34	11	4
GS-15		2.14	22	6	7	10	/	/	/	1	6	7	41	67	21	7	5
GS-16		3.15	23	4	5	7	2	/	/	1	10	10	38	65	23	7	5
GS-17		2.47	26	5	7	6	2	/	/	1	/	/	53	66	22	7	5
GS-18		1.74	42	/	15	7	12	/	/	2	1	/	21	15	8	38	39
GS-19		1.53	24	7	7	6	/	/	/	1	11	10	34	65	15	11	9
GS-20		1.27	29	10	12	3	3	/	/	/	/	/	43	72	13	9	6
GS-21		1.28	27	7	9	3	5	/	/	/	11	11	27	76	9	9	6
GS-22		1.31	34	10	12	3	7	/	/	1	/	/	33	64	18	10	8
GS-23		1.85	22	6	7	12	3	/	1	1	/	/	48	80	12	6	2
GS-24	Middle part	2.64	25	8	4	16	2	/	/	/	6	/	39	75	13	8	4
GS-25		3.05	24	6	5	17	4	/	/	/	2	/	42	52	31	12	5
GS-26		4.43	23	6	9	6	2	/	/	1	/	/	53	49	44	4	3
GS-27		2.32	18	5	6	2	6	/	2	1	/	/	60	68	21	8	3
GS-28		1.81	19	6	7	5	2	/	2	1	/	/	58	67	31	1	1
GS-29		1.66	16	2	3	31	1	/	/	/	4	2	41	93	1	4	2
GS-30		2	17	3	4	29	2	/	1	1	3	3	37	68	24	5	3
GS-31		4.24	19	4	7	24	/	/	/	/	/	1	45	66	28	3	3
GS-32		3.79	17	2	3	37	2	/	1	1	/	/	37	47	34	12	7
GS-33		1.75	27	6	9	/	/	/	/	1	/	/	57	60	29	8	3
GS-34		3.23	13	/	3	33	17	/	/	/	2	1	31	60	30	7	3
GS-35		2.16	23	5	7	12	/	/	/	1	/	/	52	59	31	7	3
GS-36		3.25	25	6	11	2	2	/	/	1	/	/	53	66	22	9	3
GS-37		3.45	26	6	9	2	/	1	/	2	/	/	54	47	45	6	2
GS-38		6.61	15	5	4	19	5	/	1	1	/	/	50	20	66	9	5
GS-39		3.25	24	6	8	9	/	/	/	1	/	/	52	43	51	4	2
GS-40	Lower part	2.96	17	8	9	9	7	/	/	2	/	/	48	59	31	6	4
GS-41		2.2	17	2	2	32	5	/	3	/	2	/	37	41	44	11	4
GS-42		1.09	29	4	8	2	1	/	/	/	1	/	55	54	33	10	3
GS-43		1.36	18	2	3	17	4	/	/	/	3	/	53	38	51	8	3
GS-44		2.01	27	3	4	5	3	/	/	1	2	/	55	69	26	3	2
GS-45		1.48	18	3	3	21	2	/	/	/	6	4	43	63	28	6	3
GS-46		1.15	32	7	10	5	15	/	/	1	/	/	30	63	21	10	6
GS-47		1.69	31	5	10	3	2	/	/	1	/	/	48	47	37	12	4
GS-48		2.89	31	5	9	5	4	/	/	1	/	/	45	65	26	6	3
GS-49		2.26	22	6	8	8	4	/	/	1	/	/	51	64	31	3	2
GS-50		2.16	20	3	3	8	2	/	/	/	5	5	54	65	21	9	5
GS-51		2.05	17	2	2	34	2	/	/	/	2	2	39	38	50	9	3
GS-52		2.21	30	5	8	18	2	/	/	2	/	/	35	53	42	3	2

(*continued on next page*)

Table 1 (*continued*)

Samples	Unit	TOC (wt.%)	Quartz (%)	Feldspar (%)	Plagioclase (%)	Calcite (%)	Dolomite (%)	Gypsum (%)	Pyrite (%)	Anhydrite (%)	Siderite (%)	Halite (%)	Clay (%)	I/S (%)	Illite (%)	Kaolinite (%)	Chlorite (%)
GS-53		3.34	19	2	4	36	2	/	/	1	2	/	34	54	34	9	3
GS-54		2.503	18	2	3	32	2	/	/	1	2	2	38	57	32	8	3
GS-55		2.02	16	2	3	37	2	/	1	1	/	2	36	59	33	6	2
GS-56		4.33	17	1	2	35	17	/	3	1	/	/	24	73	21	4	2
GS-57		2.16	10	1	2	35	31	/	2	/	1	/	18	50	14	23	13
GS-58		2.48	17	/	2	45	3	/	/	1	2	/	30	68	20	7	5
GS-59		2.81	14	2	3	30	17	/	2	/	/	/	32	44	44	8	4
GS-60		2.22	18	2	3	39	2	/	2	/	2	3	29	49	40	7	4
GS-61		1.59	23	4	8	4	/	/	/	1	/	/	60	67	29	3	1
GS-62		1.72	25	3	6	27	1	/	/	1	/	1	36	52	39	6	3
GS-63		2.08	21	3	4	33	3	/	/	1	/	2	33	39	47	9	5
GS-64		1.58	24	3	3	34	2	/	/	1	/	/	33	28	55	12	5
GS-65		1.4	23	3	2	23	5	/	/	1	/	/	43	44	43	9	4

Notes: '/' = the mineral content less than 1%; 'I/S' = Illite/Smectite.

(SEM) (red and green arrows), of which 53 samples for major and trace element measurement (red arrows).

3.2. TOC, XRD, thin sections, and SEM

All samples were measured on a LECO CS-600 total carbon and sulfur analyzer for their organic carbon contents. According to the Determination of Total Organic Carbon in Sedimentary Rocks (GB/T 19145–2003), All samples were avoided of veins, cleaned and dried. Before TOC analyses, the samples were added hydrochloric acid, and soak it for 12 h to remove the carbonate in the samples. Approximately 100 mg of powder sample was burnt in the presence of oxygen. The temperature is raised to 1050 °C. The amounts of TOC are recorded as the amount of CO_2 formed during the heating step. XRD is a method for semi-quantitative evaluation of rock mineral composition based on specific X-ray diffraction patterns of different mineral crystals. The samples were grounded into a powder less than 10 μm with an agate mortar, and gently back-pressed into a sample holder using a glass slide to smooth and flat the surface. Put the prepared samples into an X-ray diffractometer for detection, step-scanned range of 3°–45° with a step size of 0.02° (2θ). Thin section images were acquired using a polarizing Zeiss microscope. Scanning electron microscope observation was conducted on an FEI Quanta 200F, which is equipped with secondary electrons for observing the micro-morphological and structural characteristics of shale samples.

3.3. Elemental analysis

Fifty-three samples of the sixty-five samples were analyzed for their major and trace elemental composition. For major element content analysis, samples were first crushed and ground to a particle size of less than 200 mesh. The oxides of major elements of samples were determined by XRF-1800 x-ray Fluorescence Spectrometer. Samples were pre-heated at 800 °C, then mixed with Lithium tetraborate for analysis, the precision of the major element data was ≤5%. The trace element test method was based principally on the SY/T 6404-1999 standard. The experiment was conducted on an ICP-AES to obtain the trace element contents (Li et al., 2021). The samples were first ground to 200 mesh. The samples went through drying to remove organic matter and crystal water from minerals by being placed into the muffle furnace at 500 °C for 2 h. Then the processed samples were reacted with 2 ml HF, 2 ml HCI, and 6 ml HNO_3 at 185 °C for 20 min, and then transferred to the acid driver to stripe the acid at 160 °C for 90 min, and left to stand for 24 h. The element content was measured through the obtained solutions.

Based on the vertical variation characteristics of the lithology feature, the study interval was divided into the lower part, middle part, and the upper part to facilitate the discussion (Fig. 2b).

4. Results

4.1. Total organic carbon (TOC)

The TOC content of the 65 samples were presented in Table 1. The TOC content is generally greater than 1.00 *wt*%, varying from 0.87 *wt*% to 6.61 *wt*%, with an average of 2.23 *wt*% (Fig. 3a). The TOC content range from 1.09 *wt*% to 4.33 *wt*%, (avg. 2.14 *wt*%), 1.66 *wt*% to 6.61 *wt* %, (avg. 3.10 *wt*%) and 0.87 *wt*% to 3.15 *wt*% (avg. 1.71 *wt*%) in the lower part, middle part, and upper part respectively (Fig. 3b). Based on the characteristic of triple-division between the oil content and TOC of source rock (Lu et al., 2012), with references to TOC contents of 1.00 *wt* % and 2.00 *wt*%, rocks with TOC content greater than 2.00 *wt*% are defined as organic-rich rocks, with TOC content of 1.00 *wt*% to 2.00 *wt*% are defined as medium-organic rocks, and with TOC content less than 1.00 *wt*% are defined as organic-poor rocks.

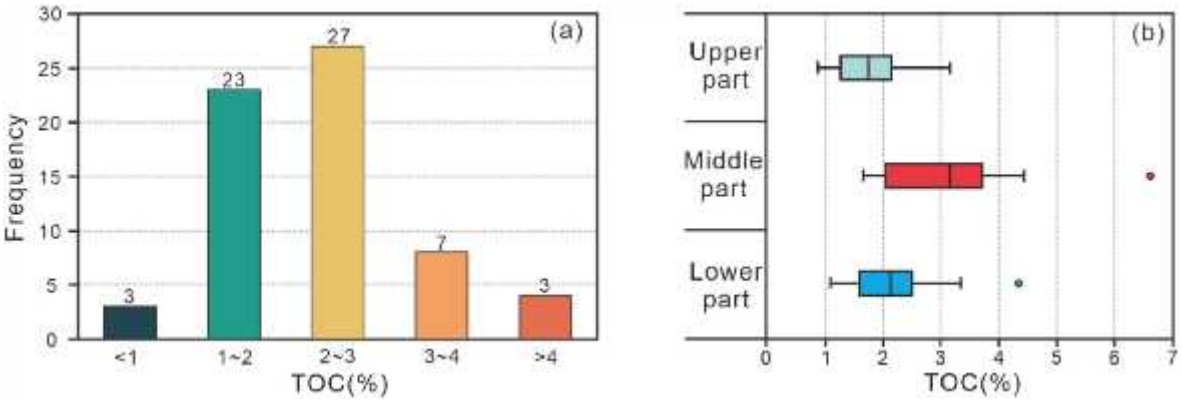

Fig. 3. (a) General distribution of TOC content in the Es_3^4 sub-member. (b) Box-plot of the TOC content in the three units of the study interval.

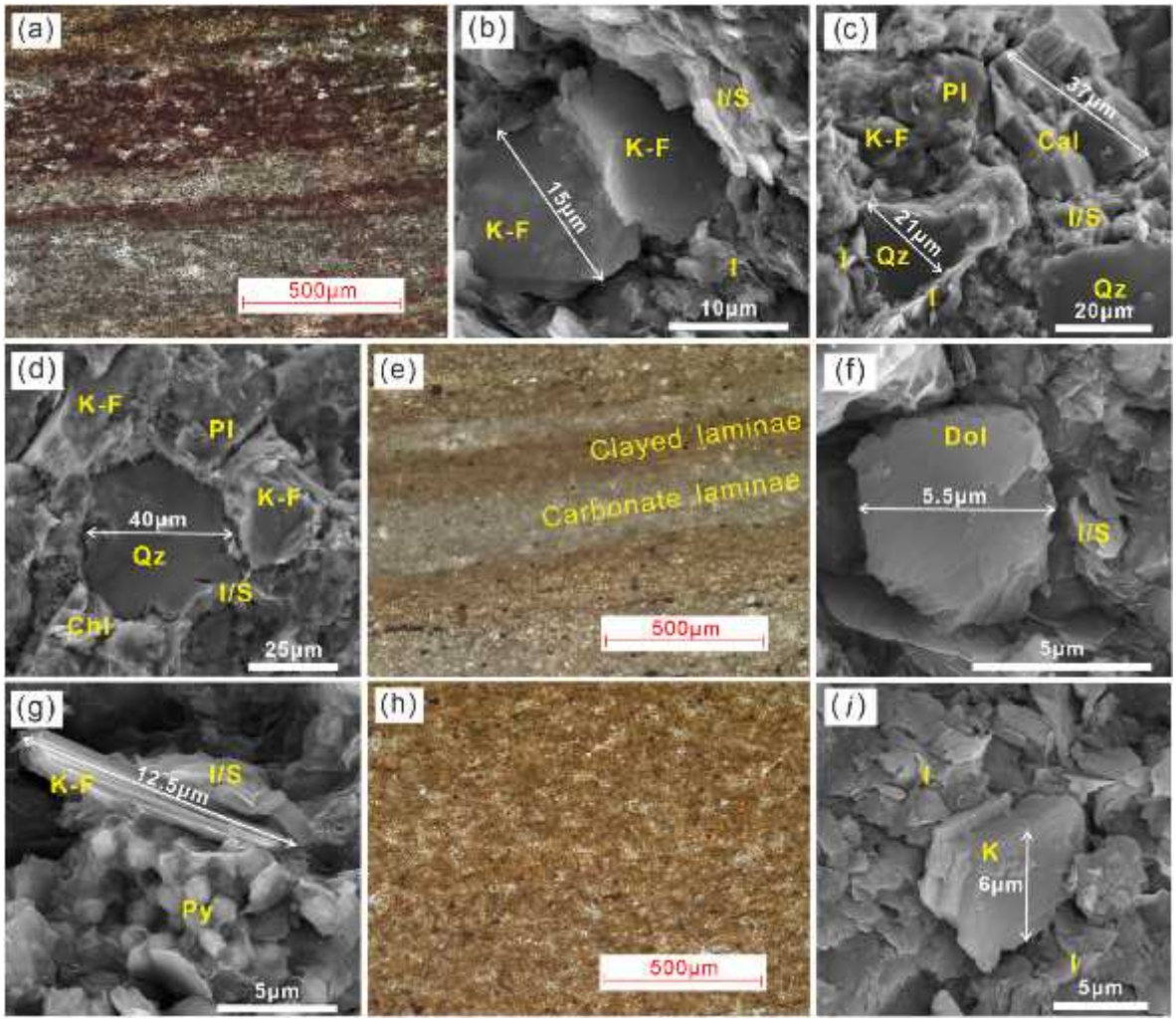

Fig. 4. Microscopic mineralogical characteristics of the shale samples in the Es_3^4 sub-member. (a) Thin section image of Clay and felsic in the GS-1 sample; (b) potash feldspar magnified from Fig. 4a; (c) SEM image of feldspar, quartz, calcite, and clay minerals in the GS-7 sample; (d) SEM image of well-rounded quartz in the GS-8 sample; (e) clay and carbonate laminae in the GS-9 sample; (f) dolomite magnified from Fig. 4e; (g) SEM image of pyrite in the GS-17 sample; (h) thin section image of clay in the GS-33 sample; (i) clay mineral magnified from Fig. 4h. K–F = potash feldspar, Pl = plagioclase, Qz = quartz, Cal = calcite, Dol = dolomite, I = illite, I/S = illite/smectite, K = kaolinite, Chl = chlorite, Py = pyrite.

4.2. Mineralogical characteristics

The XRD results are presented in Table 1. Clay minerals are the predominant mineral (avg. 41.5%) in the Es_3^4, followed by quartz (avg. 23.0%), calcite (avg. 16.8%), plagioclase (avg. 6.6%), K-feldspar (avg. 4.8%) and dolomite (avg. 4.7%), trace amounts of pyrite, gypsum, anhydrite, siderite, and halite. Clay minerals in the samples include illite-smectite, illite, kaolinite, and chlorite with average contents of 58.0%, 28.8%, 8.4%, and 4.8% respectively. The mineral is generally clay-sized (less than 39 μm), with a few silt-sized (39–62.5 μm) quartz

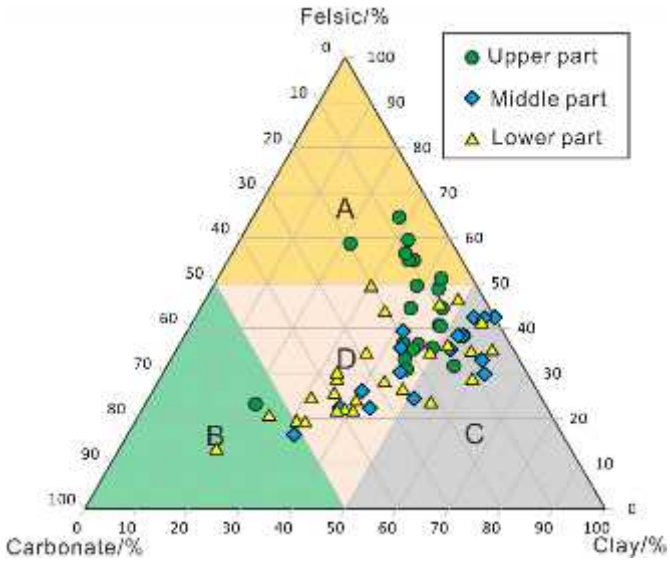

Fig. 5. Ternary plots of mineral composition of the Es_3^4 sub-member in the Nanpu Sag. Flsic = quatz + plagioclase + potash feldspar; Carbonate = calcite + dolomite. A = felsic shale, B = carbonate shale, C = clayey shale, D = mixed shale.

and feldspar in some samples (Fig. 4), and the particles are well rounded or subrounded, indicating that the particles had experienced long-distance transportation. Carbonate minerals are an aphanitic texture (Fig. 4c, e, f). Pyrite is occasionally seen under the electron microscope and is characterized by automorphic and aggregate (Fig. 4g).

According to the division scheme of fine-grained sedimentary rocks on basis of X-ray diffraction data (Chen et al., 2016a, 2016b; Jiang et al., 2013), all sample data are plotted in the ternary scatter plot (Fig. 5). The mineral content of the lower part fluctuates greatly, with the highest content of clay minerals (avg. 40.0%), followed by felsic minerals (avg. 29.3%), and the lowest content of carbonate minerals (avg. 27.6%). It is dominated by mixed shale and clayey shale, with a small amount of carbonate shale developed. The middle part is still dominated by clay minerals (avg. 47.6%), followed by felsic minerals (avg. 31.6%), with the lowest carbonate content (avg. 18.1%), and dominated by clayey shale and mixed shale. The upper part is dominated by felsic minerals (avg. 41.3%), followed by clay minerals (avg. 38.9%), with the lowest content of carbonate minerals (avg. 14.3%), and dominated by mixed shale and felsic shale.

4.3. Sedimentary structure

Based on the observations of cores and thin section identification shows that the sedimentary structure of the shale strata in the Es_3^4 sub-member can be divided into three types: laminated structure with single layers generally thinner than 1 mm (<1 mm) (Fig. 6a, b, c), layered structure with single layer greater than 1 mm and less than 10 mm (1 mm–10 mm) (Fig. 6d, e, f) and massive structure with single layers

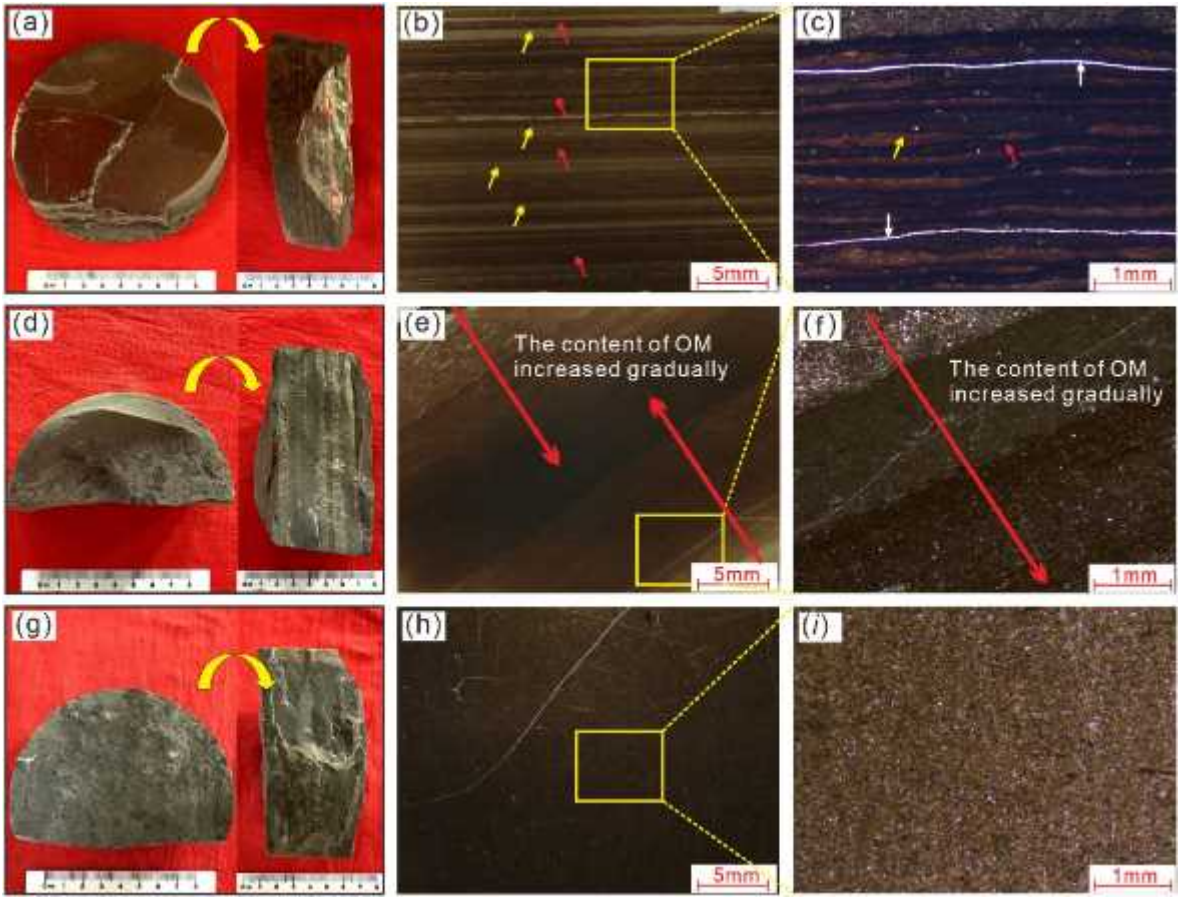

Fig. 6. Macroscopic and microscopic sedimentary structural characteristics of Es_3^4 sub-member in the Nanpu Sag. (a) (b) and (c) laminated structure, single layers generally thinner than 1 mm, yellow arrows are felsic laminae, red arrows are clayey laminae, white arrows are fractures, GS-13 sample; (d) (e) and (f) layered structure, single layers greater than 1 mm and less than 10 mm, GS-26 samples; (g) (h) and (i) massive structure, single layers greater than10mm, GS-30 sample. OM = organic matter.

Table 2
Lithofacies classification scheme of Es_3^4 sub-member in the Nanpu Sag.

Parameters	Types	Thresholds
TOC ranking	Organic-rich	TOC≥2%
	Organic-medium	2% > TOC≥1%
	Organic-poor	TOC<1%
Rock type	Felsic shale	Felsic mineral≥50%*
	Carbonate shale	Carbonate mineral≥50%
	Clayey shale	Clay mineral≥50%
	Mixed shale	All three minerals<50%
Sedimentary structure	Laminated	Single layer<1 mm
	Layered	1 mm < single layer<10 mm
	Massive	Single layer>10 mm

* The mineral content here refers to the relative content of three major categories of minerals (clay minerals, felsic minerals, and carbonate minerals).

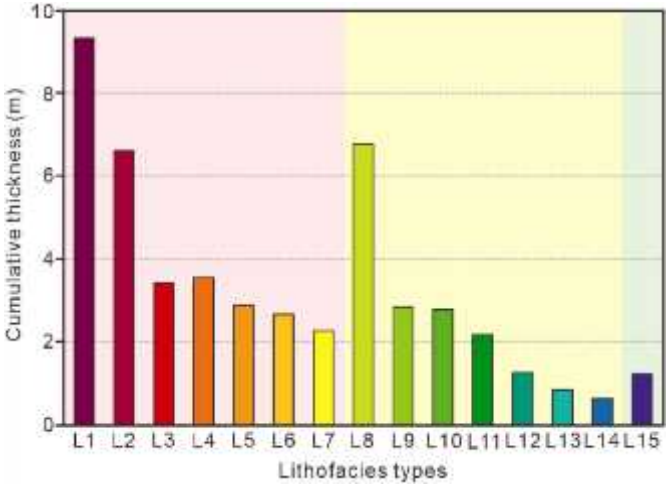

Fig. 7. Lithofacies types and their cumulative thickness of the Es_3^4 sub-member. (L1 = Organic-rich massive mixed shale, L2 = Organic-rich laminated mixed shale, L3 = Organic-rich layered clayey shale, L4 = Organic-rich massive clayey shale, L5 = Organic-rich laminated clayey shale, L6 = Organic-rich layered carbonate shale, L7 = Organic-rich layered mixed shale L8 = Organic-medium massive mixed shale, L9 = Organic-medium laminated mixed shale, L10 = Organic-medium layered mixed shale, L11 = Organic-medium massive clayey shale, L12 = Organic-medium laminated felsic shale, L13 = Organic-medium layered felsic shale, L15 = Organic-medium laminated clayey shale, L15 = Organic-poor laminated felsic shale).

greater than 10 mm (>10 mm) (Fig. 6g, h, i). The laminar structure is usually due to the difference in composition, which is manifested in the color difference. Generally, the color of felsic lamina and carbonate lamina is lighter, while clayey lamina and carbonaceous lamina is darker. The study area is dominated by clay laminae and felsic laminae (Fig. 6 b and c), with occasional carbonate laminae and carbonaceous laminae (Fig. 4e). The cumulative thickness of the laminated structure, layered structure, and massive structures are 15.45 m (accounting for 33%), 9.29 m (accounting for 17%), and 24.6 m (accounting for 50%) respectively. The laminated structure and layered structure are most developed in the upper part, and the massive structures are most developed in the middle and lower part.

4.4. Lithofacies types and their distribution

According to the observation and description of drilling cores, thin section identification, total organic carbon content analysis, and X-ray diffraction results of samples, this paper adopted the division scheme and naming method of "TOC + sedimentary structure + mineral composition" to carry out lithofacies identification and division (Table 2). The study interval is consist of 15 types of lithofacies, including seven types of organic-rich shale, seven types of organic-medium shale, and one type of organic-poor shale (Fig. 7). The three dominant lithofacies are organic-rich massive mixed shale, organic-medium massive mixed shale, and organic-rich laminated mixed shale.

The vertical variation of lithofacies is depicted in Fig. 8. Eleven types of lithofacies are identified in the lower part, the three dominant lithofacies are organic-medium massive mixed shale, organic-rich massive mixed shale, and organic-rich massive carbonate shale, together account for 66% of the lower part. The medium to rich organic matter content has good potential for shale oil exploration. Eight types of lithofacies are identified in the middle part, the three dominant lithofacies are organic-rich massive mixed shale, organic-rich layered clayey shale, and organic-rich massive clayey shale, which together account for 60% of the middle part. The highest organic matter abundance and layered structure provide a good geological foundation for shale oil exploration and development. Nine types of lithofacies are identified in the upper part, the three dominant lithofacies are organic-rich laminated mixed shale, organic-medium laminated mixed shale, and organic-rich layered mixed shale, together accounting for 57% of the upper part. The highest organic matter abundance and layered structure provide a good geological foundation for shale oil exploration and development.

4.5. Major and trace elements characteristics

Major and trace element concentrations of the Es_3^4 sub-member are presented in Table 3. The relative concentrations of some elements exhibit obvious vertical fluctuations in the study interval. The four most abundant major element oxides are SiO_2, CaO, Al_2O_3, and Fe_2O_3. Compared to the post-Archaean Australian shale (PAAS) (Taylor and Mclennan, 1985), the SiO_2, Al_2O_3, Fe_2O_3, K_2O, Na_2O, TiO_2, Cr, and V are relatively depleted, and the CaO, MgO, P_2O_5, MnO, Ba, Ni, and Sr are relatively enriched.

5. Discussion

5.1. Sedimentary environment reconstruction

The elements have different enrichment characteristics in specific environments (Mclennan, 2001). The enrichment and depletion of a series of elements reflect the specific environmental conditions of the sedimentary period. Thus, the abundance of elements and their ratios are widely used in paleoenvironmental reconstruction (Algeo and Maynard, 2004; Algeo and Tribovillard, 2009; Fedo et al., 1995; Tribovillard et al., 2006a). For a comprehensive understanding of the sedimentary environment of the Es_3^4 sub-member, the major and trace elements were adopted to interpret the paleoenvironmental. Moreover, considering the multiplicity of a single element in environmental interpretation, a combination, and a comparison of multiple parameters can improve the accuracy (Fedo et al., 1995; Nesbitt and Young, 1984; Panahi et al., 2000).

5.1.1. Paleo-climate

Titanium (Ti) and aluminum (Al) in sedimentary rocks generally exist in clay, feldspar, and other silicate minerals (Rimmer, 2004), thus Ti and Al are considered indicators of detrital flux (Li et al., 2020a, 2020b). The significant positive correlation between titanium dioxide and aluminum dioxide in the Es_3^4 sub-member indicates that these two elements are related to terrigenous input rather than authigenic (Hou et al., 2022) (Fig. 9).

The chemical index of alteration (CIA) refers to the weathering conditions of the provenance areas, and it can be used to support paleoclimate reconstruction (Nesbitt and Young, 1982). Generally, high CIAs reflect relatively humid and warm paleoclimate, whereas low CIAs suggest relatively cold and dry paleoclimate (Deer et al., 1966). The (A–CN–K) ternary diagram can reflect the trend of weathering and diagenetic alteration information (Fedo et al., 1995). Under ideal

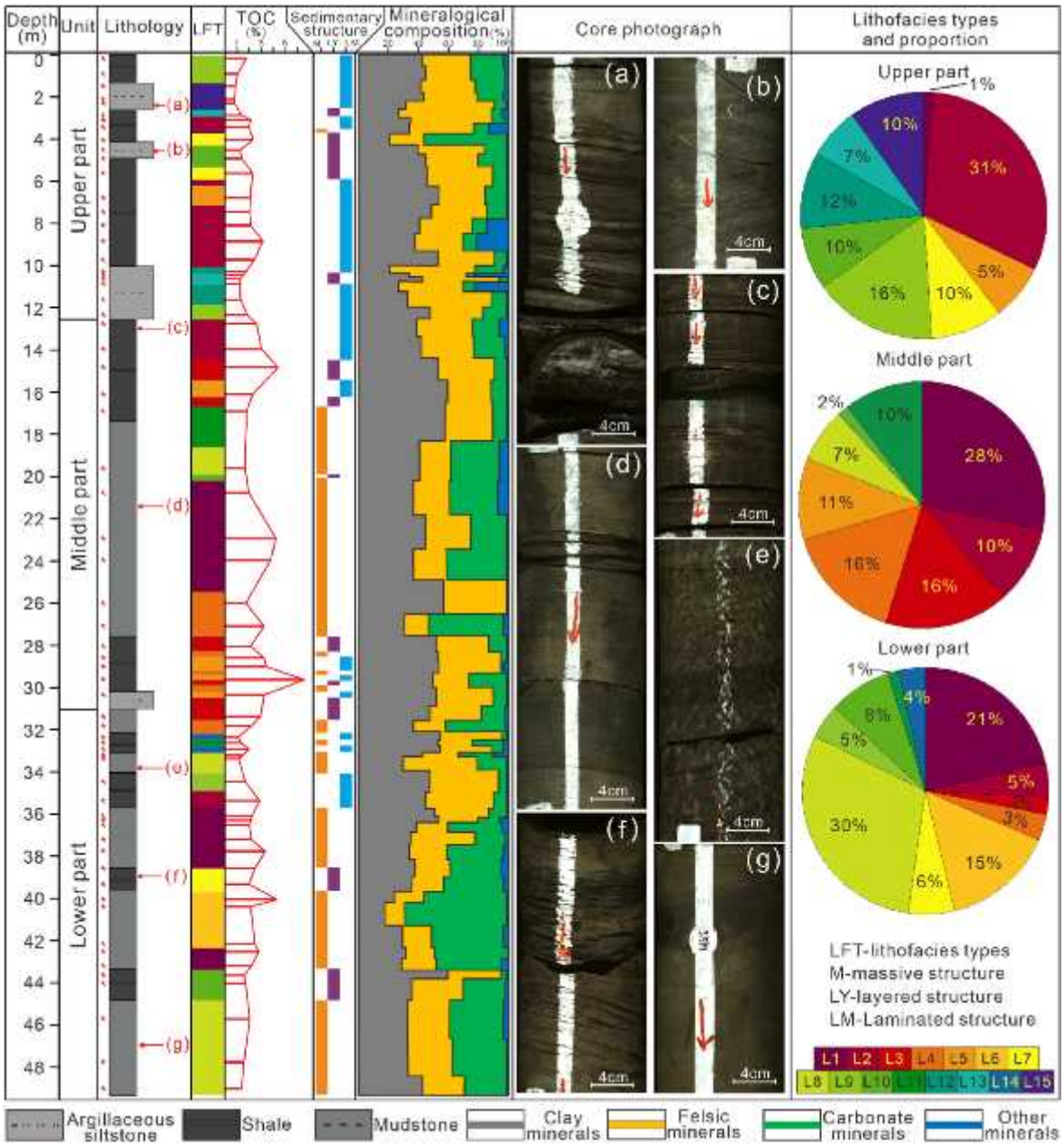

Fig. 8. The vertical variation characteristics of lithofacies in the Es_3^4 sub-member.

conditions, the weathering trend of rock should be parallel to A-CN (Nesbitt and Young, 1984; Panahi et al., 2000), but the weathering trend line of the actual sample deviates (Fig. 10), which is caused by potassium metasomatism during the weathering process (Fedo et al., 1995). We use the CIA correction formula proposed by Panahi et al. (Panahi et al., 2000) to acquire actual CIA values. Moreover, the detrital index (DI) can also reflect the terrigenous sediment flux. DI is considered to be a useful paleoclimate indicator, which is defined as follows: DI = Quartz + Feldspar + Illite + Chlorite + Kaolinite + I/S (Hou et al., 2022).

The corrected CIA values (CIAcorr) for samples from the Es_3^4 sub-member range from 14.62 to 75.70 (avg. 45.82), with mean values of 48.40, 28.62, and 55.09 for the lower, middle, and upper parts, respectively. The DI ranges from 31 to 99 (avg.75.57), with mean values of 80.22, 79.19, and 69.23 for the lower, middle, and upper parts, respectively. Indicating that the middle part was formed under a cold and arid climate along with weak chemical weathering conditions, and then a relatively warm and humid climate with a relatively strong chemical weathering occurred during the deposition of the upper part. The lower part is an evident fluctuation (Fig. 11a).

5.1.2. Paleo-salinity

Strontium (Sr) and Barium (Ba) are two elements that are regarded as empirical indicators of paleo-salinity (Liu et al., 1984; Deng and Qian, 1993; Wang, 1996). The elements Sr precipitate with an increase in salinity, and Ba precipitate with a decrease in salinity (Wei and Algeo, 2019). A high Sr/Ba ratio reflects high salinity, and a low Sr/Ba ratio indicates low salinity. The CaO content of the samples from the Es_3^4 sub-member range from 1.12% to 35.24% (avg. 13.62%), indicating the presence of carbonate in the Es_3^4 sub-member. However, a significant positive correlation between Sr contents, Sr/Ba ratios, and CaO contents is found (Fig. 12a and b), illustrating the Sr and Ba content didn't affect by high carbonate content (Wei and Algeo, 2019). Therefore, the Sr/Ba ratio of all samples can be used to estimate the salinity. The Sr/Ba ratios of the samples from the Es_3^4 sub-member vary from 0.50 to 2.35 (avg.

Table 3
Major and trace element concentrations of the samples in the Es_3^4 sub-member.

Samples	Unit	SiO_2	CaO	Al_2O_3	Fe_2O_3	K_2O	Na_2O	TiO_2	P_2O_5	Al	Ba	Ca	Cr	Fe	Mn	Ni	Sr	V
		(%)	(%)	(%)	(%)	(%)	(%)	(%)	(%)	(μg/g)	(μg/g)	(μg/g)	(μg/g)	(μg/g)	(μg/g)	(μg/g)	(μg/g)	(μg/g)
GS-1	Upper part	46.32	15.78	12.33	8.03	2.20	0.93	0.69	0.95	8.44	731.6	6.854	91.65	4.273	3588	286.8	554.5	79.39
GS-2		54.14	9.47	14.01	6.71	2.76	1.10	0.73	0.91	7.772	651.7	9.774	101.7	5.669	1765	221.7	617.8	75.44
GS-3		52.09	10.64	13.63	6.98	2.59	1.09	0.73	0.66	8.888	710.4	7.091	106.1	4.621	1473	150.9	537.4	88.42
GS-4		50.69	11.41	13.12	8.07	2.49	1.08	0.71	0.83	8.763	737.8	8.323	107.4	5.112	1822	306.8	522.1	93.23
GS-6		64.19	4.20	11.82	5.94	2.53	1.84	0.38	0.18	6.829	838.1	5.129	73.94	5.703	982.7	195.9	452.7	40.43
GS-7		60.39	6.20	13.03	5.24	2.71	1.55	0.77	0.17	8.057	824	4.422	87.3	4.115	602.5	458.7	409.8	97.5
GS-8		60.30	4.25	14.06	5.34	3.01	1.73	0.80	0.69	8.046	706	5.86	87.41	3.717	742.9	110	502.5	77.5
GS-9		60.44	4.36	14.05	5.50	3.02	1.70	0.74	0.41	9.209	747.6	3.307	87.78	3.14	391.5	184	445.6	87.74
GS-10		57.04	8.35	13.52	4.73	2.54	1.87	0.76	0.57	8.201	729.4	6.478	75.06	3.386	662	63.22	575.8	73.76
GS-11		58.81	5.38	14.30	5.19	2.87	1.66	0.83	0.48	8.765	790.6	3.27	74.11	3.152	868.6	194.9	476.7	87.88
GS-12		58.67	5.35	14.27	4.94	2.78	1.77	0.78	1.07	8.807	835.1	3.131	70.72	3.36	342.8	281.7	505.1	84.63
GS-13		51.84	9.56	15.18	6.35	2.91	1.05	0.75	0.81	8.026	867.4	7.856	97.07	5.196	945.4	257.9	789.4	68.16
GS-14		51.57	10.21	14.39	7.96	2.71	1.11	0.73	0.77	8.973	784	6.073	98.42	4.432	851.9	111.2	536.7	82.92
GS-16		48.36	10.23	12.47	13.26	2.29	1.00	0.63	0.91	7.317	699.9	9.025	129.4	9.757	2434	808.3	560	59.96
GS-17		58.17	6.02	13.58	7.50	2.76	1.32	0.69	0.91	9.119	832.7	5.216	94.89	4.364	816.2	167.6	508.9	74.66
GS-20		63.26	4.16	13.03	4.84	2.58	1.63	0.71	0.29	7.894	819.9	2.427	57.28	3.072	442.9	124.1	421.6	69.73
GS-22		62.07	4.87	12.95	4.67	2.74	1.72	0.66	0.43	8.065	843.2	3.001	52.27	2.868	474.4	34.64	508.3	66.39
GS-23		59.96	1.69	17.40	4.97	3.50	1.33	0.77	0.63	10.1	729.3	1.295	96.71	3.584	178.5	434.6	427.3	92.1
GS-24	Middle part	39.69	19.51	10.58	11.37	1.87	0.75	0.49	0.67	8.031	800.1	11.85	94	4.39	1340	498.9	891.2	66.59
GS-26		34.31	25.35	7.07	15.43	1.08	0.52	0.36	0.66	4.766	706.2	18.41	113.7	9.213	2921	54.87	1014	38.13
GS-27		45.51	17.94	12.63	6.54	2.17	0.91	0.64	0.49	8.412	755	11.52	81.44	3.209	824.4	537.4	693.1	67.36
GS-28		34.89	26.41	9.41	8.77	1.54	0.66	0.42	0.85	5.523	703.2	18.03	79.96	5.068	1586	77.24	886.8	42.29
GS-30		41.78	18.15	10.46	11.75	1.79	0.72	0.45	0.76	7.497	734.4	11.11	99.94	5.852	2088	100.4	741.6	57.1
GS-31		39.97	22.24	9.82	10.27	1.59	0.65	0.47	0.78	4.475	508.3	14.07	75.08	5.061	2321	36.54	838.6	35.37
GS-32		45.17	20.88	11.81	5.17	2.03	0.84	0.58	0.77	7.99	829.9	8.557	74.24	3.236	675.4	474.7	682.3	65.98
GS-33		44.84	16.06	10.86	9.56	1.99	0.78	0.54	1.32	5.371	640.4	10.38	91.19	5.115	1288	197.8	906.6	43.72
GS-34		34.17	27.04	8.25	9.25	1.38	0.76	0.36	1.42	3.825	525.5	16.09	67.22	4.517	1348	47.38	734.7	29.52
GS-35		33.94	30.44	8.52	6.34	1.48	0.63	0.41	1.41	5.531	626.2	13.7	60.9	2.485	774.9	48.58	850	42.34
GS-36		34.82	27.06	9.18	7.17	1.56	0.61	0.44	1.47	3.73	740.2	17.67	52.95	2.777	930.8	7.994	1011	28.91
GS-37		47.45	15.26	14.19	4.78	2.14	1.13	0.75	0.80	8.403	772	5.512	69.08	2.558	346	815.9	576.1	76.75
GS-38		32.90	31.17	5.56	9.86	0.88	0.45	0.28	1.98	2.576	436.4	17.48	66.07	4.894	1421	42.57	903.1	22.69
GS-40	Lower part	62.45	1.12	17.85	3.22	3.41	1.20	0.87	0.26	9.84	623.9	0.8604	84.13	1.992	145.6	532.4	348.6	89.85
GS-41		39.82	22.67	10.90	6.75	1.82	0.66	0.48	1.25	4.965	652.3	14.07	64.86	3.577	810.4	309.9	843.4	38.46
GS-42		58.36	6.14	15.74	3.77	2.88	1.14	0.85	0.52	9.666	594.5	0.824	84.13	2.015	181.5	172.4	338.4	91.51
GS-43		46.48	15.75	13.10	6.66	2.29	0.64	0.61	0.75	7.261	661.1	8.953	78.96	3.273	618.3	342	632.8	58.85
GS-44		59.74	2.49	17.41	4.57	3.36	1.15	0.80	0.70	9.908	656.8	1.201	92.35	2.964	157.5	15.01	385.8	81.55
GS-46		60.97	6.49	12.90	4.84	2.42	1.26	0.73	0.42	7.208	672.9	4.454	57.22	2.708	494.7	134	342.5	63.01
GS-47		62.15	2.72	16.68	3.42	2.99	1.11	0.88	0.44	8.773	558.4	1.116	134.3	2.167	250.2	55.43	300.4	90.4
GS-48		59.73	3.02	16.07	5.10	2.98	1.01	0.77	0.97	9.053	659.2	2.179	86.04	3.336	255.8	187.4	350.1	80.36
GS-49		47.93	12.54	11.81	12.32	1.93	0.66	0.53	0.57	6.594	576.2	8.999	93.42	5.315	1217	106.2	558.8	52.49
GS-51		56.81	9.07	13.74	4.85	2.29	0.90	0.79	0.42	6.264	488.1	8.917	74.67	3.337	687.2	122.1	455.3	63.17
GS-53		48.50	12.60	13.62	9.33	2.18	0.75	0.57	0.38	6.607	533.7	9.328	100.5	5.525	1157	220.8	510.3	57.81
GS-55		62.12	1.65	17.75	3.12	3.11	1.33	0.85	0.31	8.66	501.2	3.977	90.16	2.639	274.8	353.1	433.6	85.21
GS-56		29.75	35.24	6.59	7.28	1.02	0.43	0.32	1.22	2.903	328.5	18.73	60.05	3.677	963.1	14.81	772.8	25.22
GS-57		28.51	33.84	7.26	8.05	1.06	0.46	0.34	0.88	3.763	424.4	15.98	49.31	2.666	838.8	38.55	801	28.98
GS-58		39.85	24.84	11.23	5.85	1.54	0.60	0.62	0.91	3.509	361.1	16.26	52.6	3.014	735.6	21.58	764.9	30.33
GS-59		38.94	22.67	11.36	7.68	1.74	0.63	0.52	1.11	5.832	439.9	11.94	66.77	3.376	702.4	149.3	485.9	46.95
GS-60		44.13	19.93	11.56	7.99	1.85	0.72	0.57	1.05	5.808	477.8	11.95	69.62	3.6	754	35.43	575.1	48.59
GS-61		55.78	7.42	16.73	4.20	2.36	1.16	0.75	0.35	8.513	617.9	4.502	75.49	2.573	268.7	167.5	432.2	74.51
GS-62		54.50	7.48	16.46	4.83	2.78	0.93	0.81	0.57	9.716	684.1	1.482	86.5	3.01	147.6	250.8	375.5	90.54
GS-63		49.36	15.11	13.10	5.61	2.34	0.62	0.63	0.65	6.729	535.2	9.565	68.57	2.851	567	270.4	465.7	55.05
GS-64		43.15	16.77	11.20	10.99	1.88	0.65	0.53	1.83	6.062	497.8	9.423	88.4	4.647	949.3	277	455.6	48.29
GS-65		51.77	12.58	13.11	6.27	2.38	0.64	0.70	0.42	7.378	500.8	7.072	71.06	2.87	482.8	159.7	413	62.46

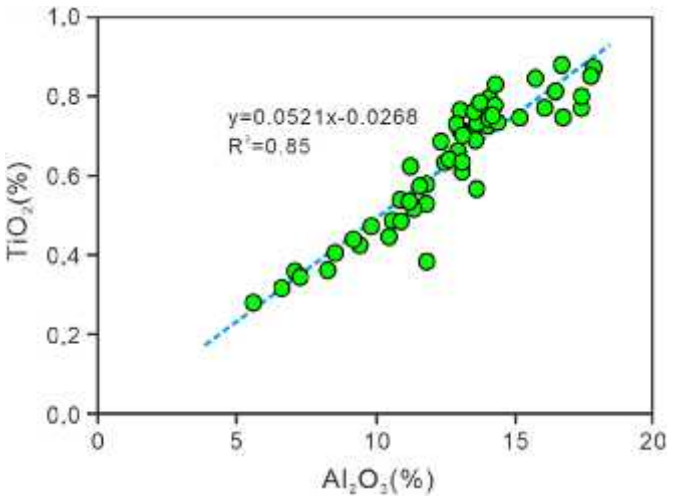

Fig. 9. Correlation between TiO_2 and Al_2O_3 of the shales associated with the Es_3^4 sub-member.

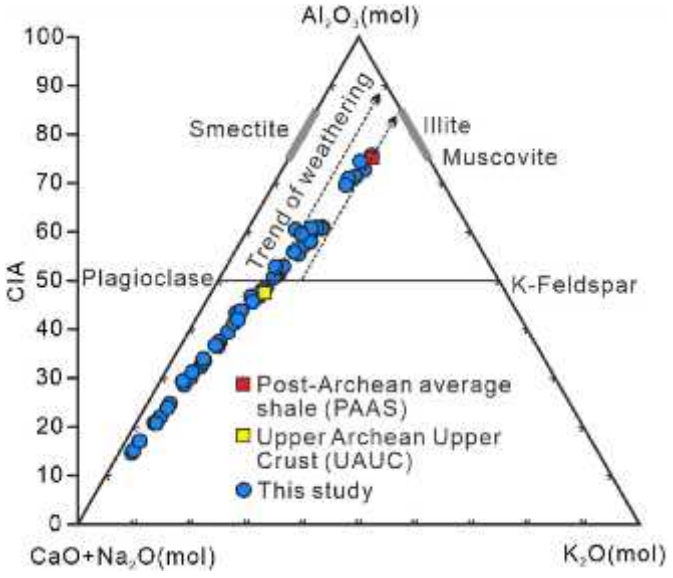

Fig. 10. The A–CN–K ternary diagram of the Es_3^4 sub-member. PAAS values after Taylor and Mclennan (1985). UAUC values after Condie, 1993. The dashed arrows represent an ideal chemical weathering trend.

0.95), with mean values of 1.02, 1.23, and 0.68 for the lower, middle, and upper parts, respectively, suggesting that the shale samples were deposited in a brackish-salt water environment (Fig. 11b).

The relative proportion of iron (Fe) and calcium (Ca) are sensitive to water salinity, and the Ca/(Ca + Fe) ratios in fine-grained sediments can be used to distinguish salinity change (Nelson, 1967). The Ca/(Ca + Fe) ratios of the samples from the Es_3^4 sub-member vary from 0.27 to 0.86 (avg. 0.62), with mean values of 0.66, 0.70, and 0.54 for the lower, middle, and upper parts, respectively, also indicating a high saline water condition during deposition of the Es_3^4 sediments (Fig. 11b). A combination and comparison of multiple parameters can improve the accuracy of the determination. The Ca/(Ca + Fe) ratios versus Sr/Ba ratios suggest that the upper part is brackish-fresh water, the middle part is salt-brackish water, and the lower part is an evident fluctuation among salt, brackish, and freshwater (Fig. 12c).

5.1.3. Paleo-productivity

Organic-rich sediments generally contain high organic carbon and authigenic nutrient elements, the enrichment of these elements can be completed through the uptake of biological nutrients and the adsorption of metal elements (Piper and Calvert, 2009). Phosphorus (P) is an important nutritional element, which can greatly control the paleo-productivity of marine and lacustrine shales (Tyrrell, 1999). Both modern and ancient sedimentation studies show that there is a good positive correlation between the content of barium and the flux of organic carbon in sediments (Francois et al., 1995; Paytan and Griffith, 2007; Griffith and Paytan, 2012). Therefore, the accumulation rate or content of Phosphorus and Barium in sediments are good indicators of the primary productivity of ancient sediments (Latimer and Filippelli, 2002; Qiu et al., 2021).

To reduce the influence of authigenic minerals and organic matter on the dilution of P and Ba, P/Al and Ba/Al are more effective in assessing paleo-productivity (Algeo and Tribovillard, 2009; Chen et al., 2016a, 2016b; Latimer and Filippelli, 2002). The highest TOC content and the highest concentration of P/Al and Ba/Al in the middle part, and the lowest TOC content and the lowest concentration of P/Al and Ba/Al in the upper part and the lower part (Fig. 13a), indicate that the paleo-productivity has a significant impact on organic matter accumulation.

5.1.4. Paleo-redox

V/(V + Ni) and V/Cr are widely used for reconstructing paleo-redox. However, vanadium (V) may not be trapped in the rocks by iron sulfide in the strata with minimal detrital influences (Algeo and Maynard, 2004) and may be removed from pore water below the reduction level of manganese-iron-oxide (Morford, 1999). The complexity of chromium (Cr) migration and enrichment limits its paleoenvironmental reconstruction in the strata with minimal strong detrital influences (Tribovillard et al., 2006b). In the target strata with a marked change in terrigenous input, thus the parameters such as V/(V + Ni) and V/Cr can not be used to analyze paleo-redox effectively.

On the other hand, the enhanced ability of sediment to remove Fe under anoxic and euxinic conditions, thus Fe/Al ratios commonly increase under reducing conditions (Clarkson et al., 2014; Li et al., 2020a, 2020b; Raiswell and DE Canfield, 1998; Timothy et al., 2006). The Fe/Al ratios of the Es_3^4 sub-member range from 0.2 to 1.93 (avg. 0.62), with means values of 0.53, 0.92, and 0.54 for the lower, middle, and upper parts, respectively, suggesting a predominantly anoxic water environment during the Es_3^4 sub-member, and an evident fluctuation between oxic and anoxic water environments during the lower part and upper part (Fig. 13b).

Many element geochemical indexes are based on statistics to distinguish redox conditions, so more evidence needs to be found from sedimentary geology (Algeo and Li, 2020; Qiu et al., 2021). Fossils and pyrite in the Es_3^4 sub-member are two good pieces of evidence of paleo-redox conditions. There are complete and broken burial plant fossils in the middle part, these are preserved along the bedding plane (Fig. 14a and b). The complete leaf fossil may not be subject to strong hydrodynamic action during burial, reflecting the semi-deep to deep lake environment of low oxygen. Moreover, with enough growth space, the pyrites formed in the sedimentation period easily form strawberry aggregates with a regular shape (Wang et al., 2012). The size of pyrites in deposits is also indicative of redox conditions in the sedimentation period, the pyrites with small grain diameter (less than 15 μm) are generally formed in an oxygen-deficient environment (Loucks et al., 2012). According to scanning electron microscope observation, the diameter of the pyrites less than 12 μm are widely developed in the middle and lower parts (Fig. 14c and d), and there is a good positive correlation between pyrite content and reduction degree (Fig. 13b).

5.2. Sedimentary environment controls lithofacies development

5.2.1. Sedimentary environment controls the abundance of organic matter

The relationship between TOC content and paleo-productivity,

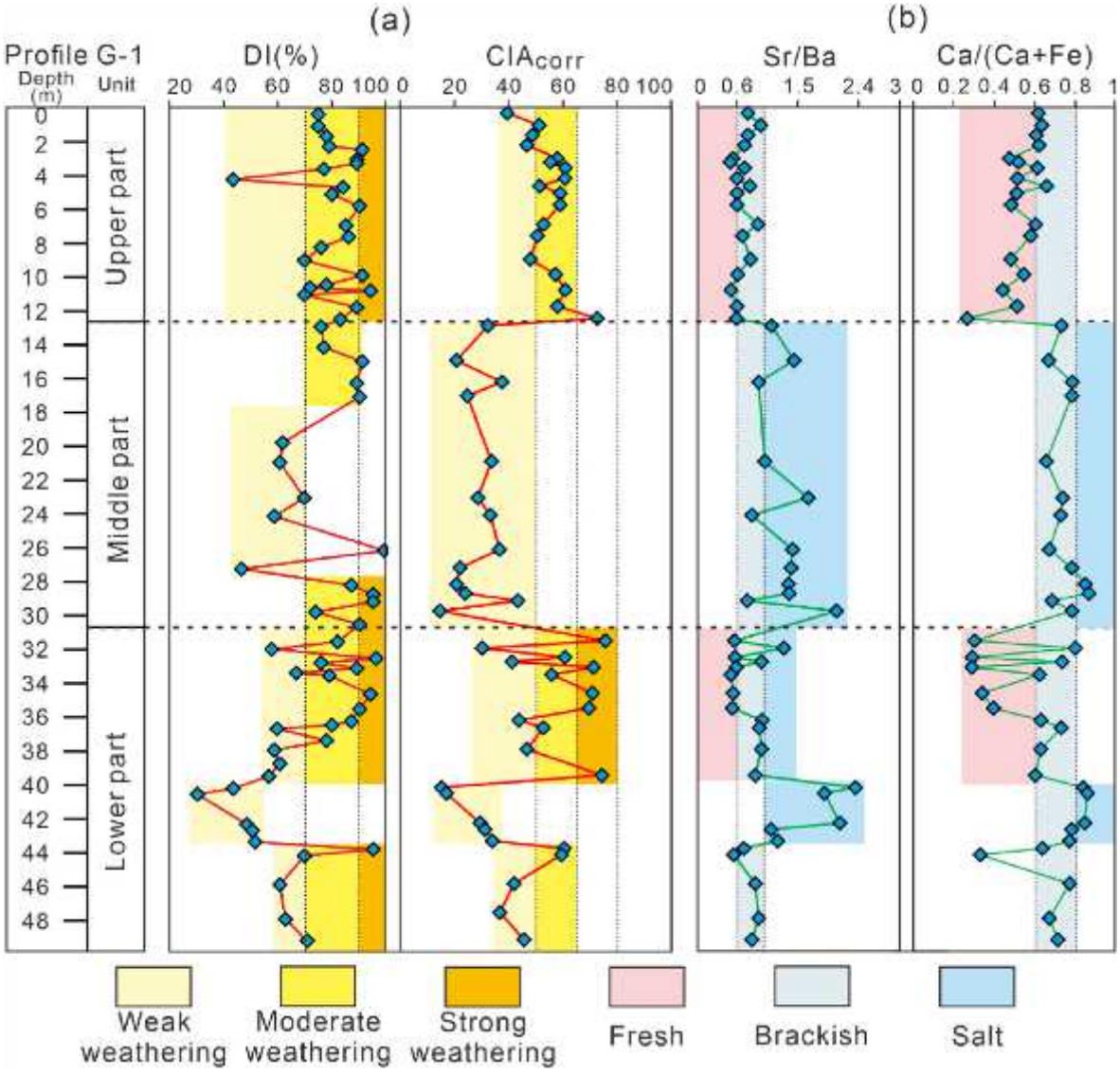

Fig. 11. (a) The detrital index (DI) and chemical index of alteration (CIA) profile of the Es_3^4 sub-member; (b) the Sr/Ba and Ca/(Ca + Fe) profile of the Es_3^4 sub-member.

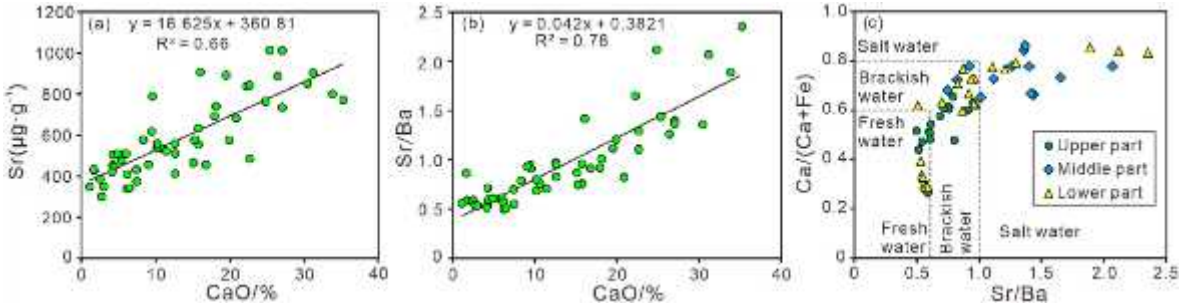

Fig. 12. Illustrations of paleoenvironment characteristics of the Es_3^4 shales. (a) Correlation between Sr and CaO, after (Wei and Algeo, 2019). (b) Correlation between Sr/Ba and CaO. (c) Ca/(Ca + Fe) ratios versus Sr/Ba ratios showing the depositional environment, adopted after (Ma et al., 2022).

paleo-climate conditions, paleo-salinity, and paleo-redox conditions was analyzed. It can be seen that TOC content has a significant positive correlation with P/Al, Ba/Al, and Fe/Al; With the increase of CIA value, TOC content decreased first and then increased; With the increase of Sr/Ba and Ca/(Ca + Fe) value, TOC content first showed a plateau period. When Sr/Ba and Ca/(Ca + Fe) increased to 0.6, TOC increased with the increase of their ratio (Fig. 15), indicating that the paleo sedimentary environment had obvious control over the abundance of organic matter.

Based on the above research on the relationship between geochemical parameters, it is speculated that the enrichment of organic matter in the Es_3^4 sub-member in Nanpu Sag is controlled by primary productivity, terrigenous input, and preservation conditions. Paleo-productivity

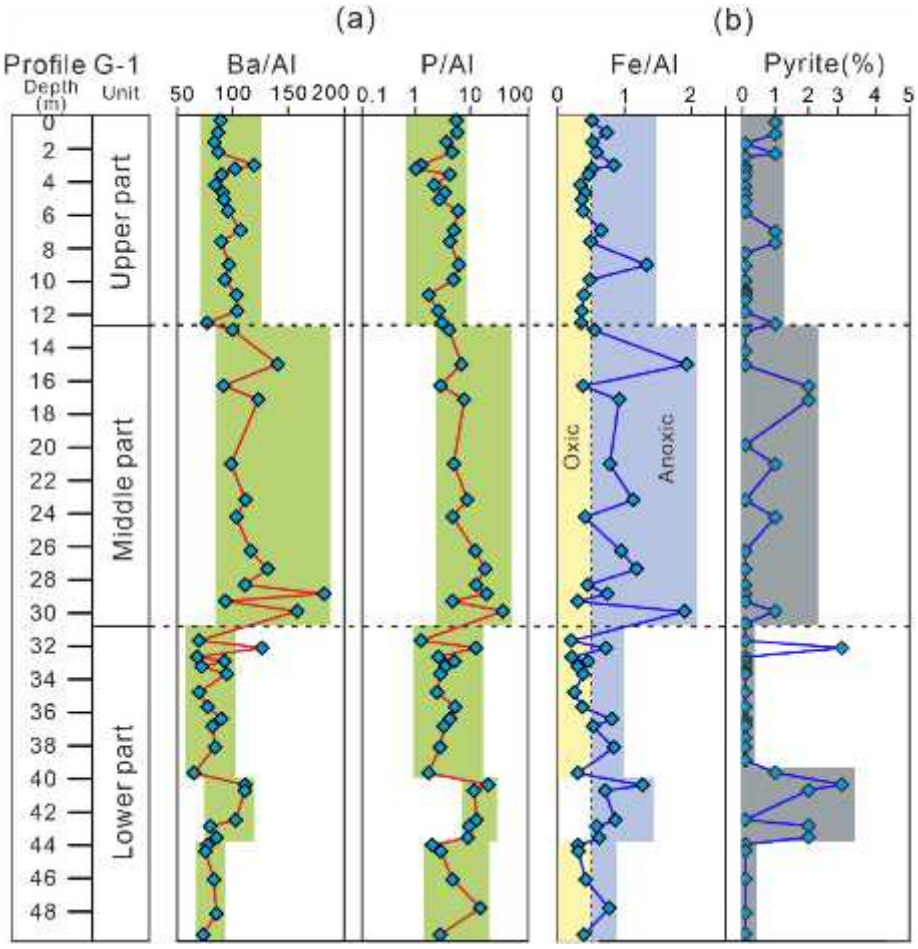

Fig. 13. (a) The Ba/Al and P/Al profile of the Es_3^4 sub-member. (b) The Fe/Al and pyrite profile of the Es_3^4 sub-member.

conditions and redox conditions are necessary conditions for the enrichment and preservation of organic matter (Hou et al., 2022; Qiu et al., 2021; Kassem et al., 2022). Therefore, high production and strong reduction conditions play a good role in promoting the enrichment of organic matter with an obvious positive correlation (Fig. 15a, b, f). The increase in surface runoff not only brings a large amount of oxygen-enriched freshwater but also brings a large number of nutrients. When the local surface runoff is small, it has a stronger destructive effect on the enrichment of organic matter. With the increase of terrigenous input (CIA >50), the promoting effect is greater (Fig. 15c). In addition, when the water supply in the basin is less than the evaporation, the water salinity increases. The increase in water salinity is conducive to improving primary productivity and forming an anoxic environment, which also promotes the enrichment of organic matter (Fig. 15d and e).

The sedimentary environment of the lower part fluctuates obviously. The increase of short-term surface runoff replenishes the oxygen in the water body and destroys the reduction conditions of the water body. The low terrigenous input in the dry and cold climate increases the salinity of the water body. The appropriate salinity is conducive to the formation of biological reproduction and reduction conditions, which promotes the enrichment and preservation of organic matter. During the sedimentary period of the middle part, the climate conditions are the driest, and the weathering degree of the provenance area and the DI in the sediment are the lowest. A large amount of water evaporation makes the salinity of the lake rise significantly, the productivity and reduction conditions are the strongest, and a large amount of organic matter is enriched to form shale with high organic matter abundance. The climate of the upper part was the wettest, the weathering degree of the provenance area was high, the salinity of the water body was low, and the productivity and reduction conditions were relatively weakened. At this time, the terrigenous input promoted the enrichment of organic matter, however, the oxic conditions make most of the organic matter to be decomposed.

5.2.2. *Sedimentary environment controls the mineral composition*

The mineral composition of shale in continental lakes shows a variety of transport sedimentary characteristics, which reveals the complexity of the fine-grained sedimentary process. The most common clay minerals and felsic minerals are mostly derived from the weathering products of the parent rock and belong to terrigenous clastic components (Jiang et al., 2013; Krumbein, 1933; Potter et al., 2005). Among them, clay minerals are mainly transported to the catchment basin by suspension, which needs to be settled by flocculation (Curran et al., 2002; Eisma, 1986; Krumbein, 1933), and felsic minerals are mainly mechanically deposited (Pan et al., 2014; Tripsanas et al., 2007). Carbonatite minerals in continental lake basins are usually related to the salt-brackish water sedimentary system (Flügel, 2010). The bottom water rich in calcium carbonate circulates into the surface water in the wet season, and the salinity of the water body increases continuously in the dry season, to precipitate and form carbonate-rich strata (Shinn et al., 1993; Schieber et al., 2013; Zhang et al., 2017).

Under warm and humid climate, rocks are more prone to weathering and mineral transformation, and weathering products and minerals with strong weathering resistance are deposited after long distance transportation (Nesbitt et al., 1996). In this study, the weathering degree of provenance area is positively correlated with clay and felsic minerals, while negatively correlated with carbonate minerals (Fig. 16a, c, e). In addition, water salinity is negatively correlated with clay minerals and felsic minerals, while it is positively correlated with carbonate minerals

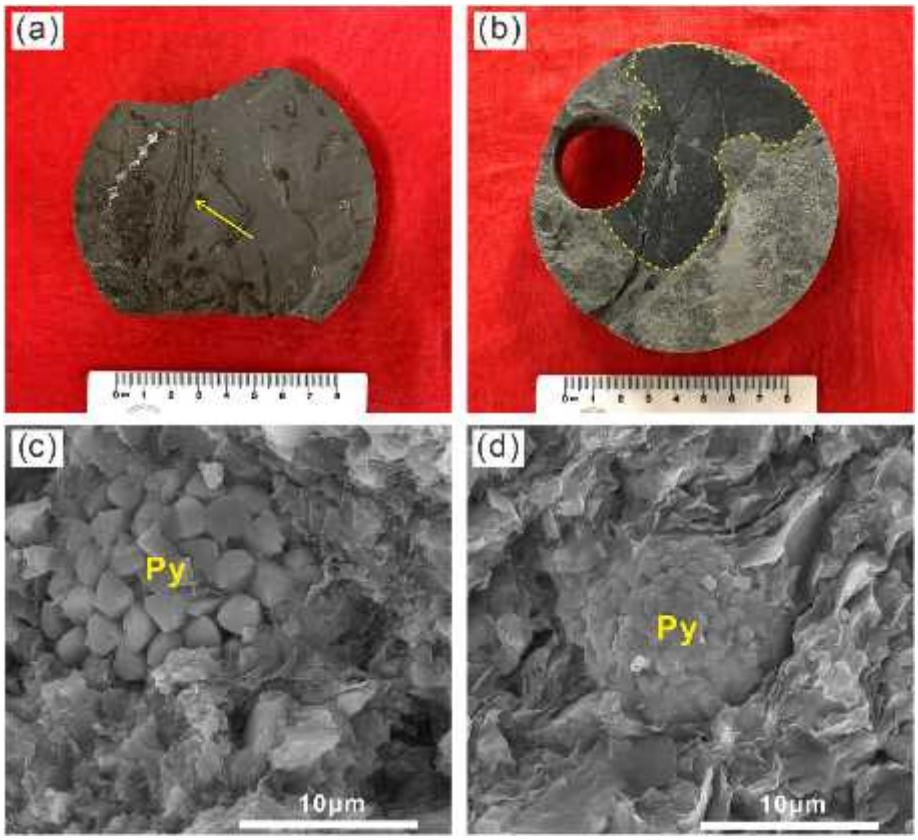

Fig. 14. Core photographs and SEM images of shale in Es_3^4 sub-member. (a) and (b) Fossils of branches and leaves in the middle part. (c) and (d) Strawberry aggregates with the regular shape of pyrites (Py) in the lower part.

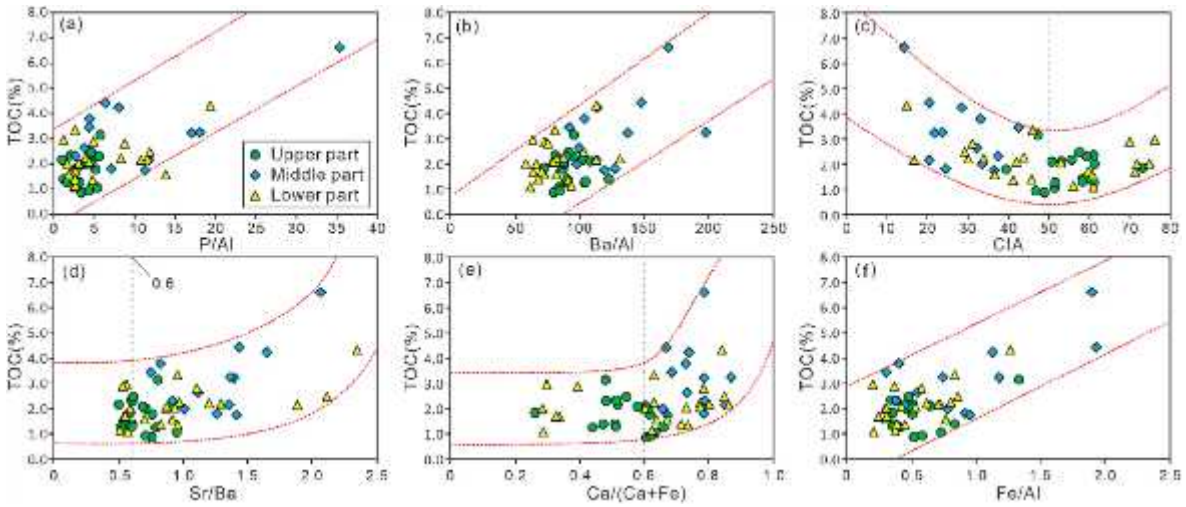

Fig. 15. The relationship between TOC and sedimentary environment.

(Fig. 16b, d, f). The results show that during the sedimentary period of the Es_3^4 sub-member, the rock and mineral composition is affected by paleo-climate and paleo-salinity. The lower part and upper part with relatively warm and humid conditions, the content of clay and felsic minerals in the sediments is higher and the content of carbonate minerals is lower; The sediments in lower and middle part of the investigated interval are suggested to be deposited under relatively cold and arid conditions, as reflected by the low content of clay and felsic minerals as well as abundance of carbonate.

5.2.3. Sedimentary environment controls the laminae development

The components of laminae in the Es34 sub-member are mainly organic-rich clay laminae and felsic laminae, and a small number of carbonate laminae are developed in the lower part, while the organic-rich clay laminae and felsic laminae in the upper part corresponding to the strong weathering conditions of relatively high CIA and high DI, as well as the low salinity conditions of relatively low Sr/Ba and Ca/(Ca + Fe). Carbonate laminae correspond to weak weathering conditions with relatively low CIA and low DI, and high salinity conditions with relatively high Sr/Ba and high Ca/(Ca + Fe) (Fig. 17a and b).

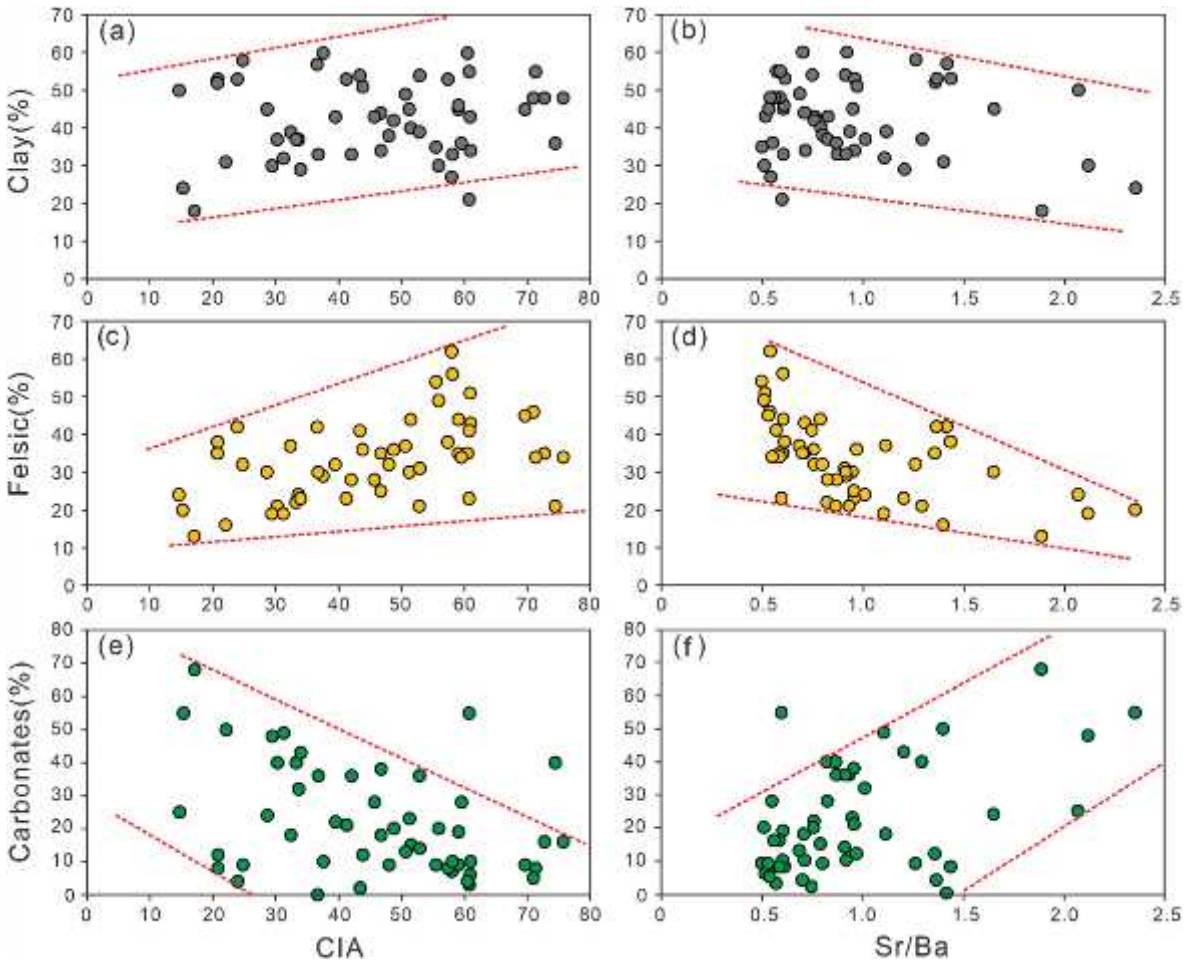

Fig. 16. The relationship between mineral contents and paleoenvironment. (a) Clay content versus CIA; (b) clay content versus Sr/Ba; (c) felsic content versus CIA; (d) felsic content versus Sr/Ba; (e) carbonates content versus CIA; (f) carbonates content versus Sr/Ba.

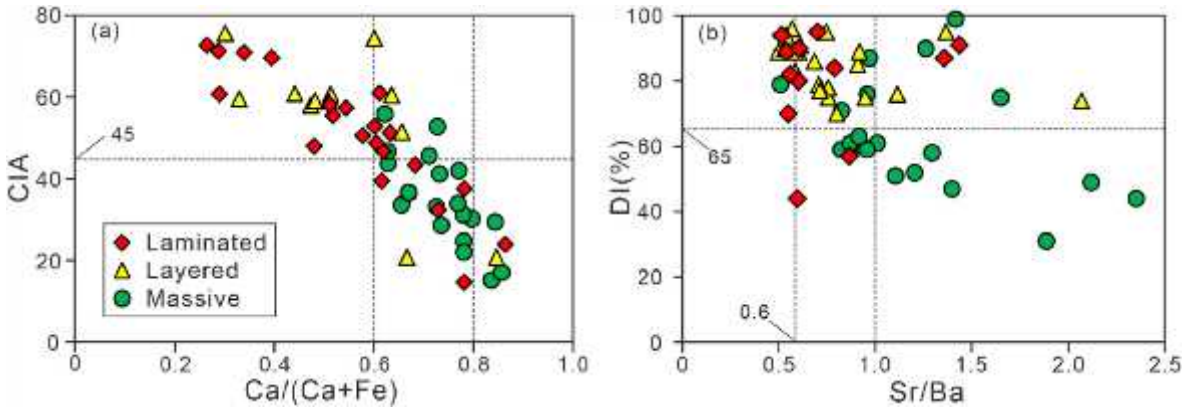

Fig. 17. Relationships among the shale paleo-weathering, paleo-salinity, and sedimentary structure. (a) Sr/Ba versus CIA and sedimentary structure. (b) Ca/(Ca + Fe) versus DI and sedimentary structure.

At present, it is widely considered that on the premise of stable tectonic background, the climate cycle is the most extensive controlling factor for laminae formation (Anderson and Dean, 1988; Zolitschka et al., 2015). Because no matter the stratification of the water, the injection of water flow, or the factors affecting the formation of laminae such as salinity, water depth, and biological activities are closely related to climate. The common formation mechanisms of lacustrine shale laminae include water transport and differentiation (Schieber et al., 2007; Yawar and Schieber, 2017; Yuan et al., 2015), terrestrial seasonal input (Li et al., 2015; Zolitschka et al., 2015), the seasonal bloom of algae (Liu et al., 2001; Walker et al., 1999; Wang and Zhong, 2004), water stratification (Håkanson et al., 1989; Li et al., 2020a, 2020b; Negri, 1996) The preservation conditions of laminae are closely related to the water depth and the degree of water stratification (Li et al., 2020a, 2020b).

Under warm and humid conditions, the source area is strongly weathered. The river carries a large amount of terrigenous clastic materials into the lake, which makes the sediments contain a large amount

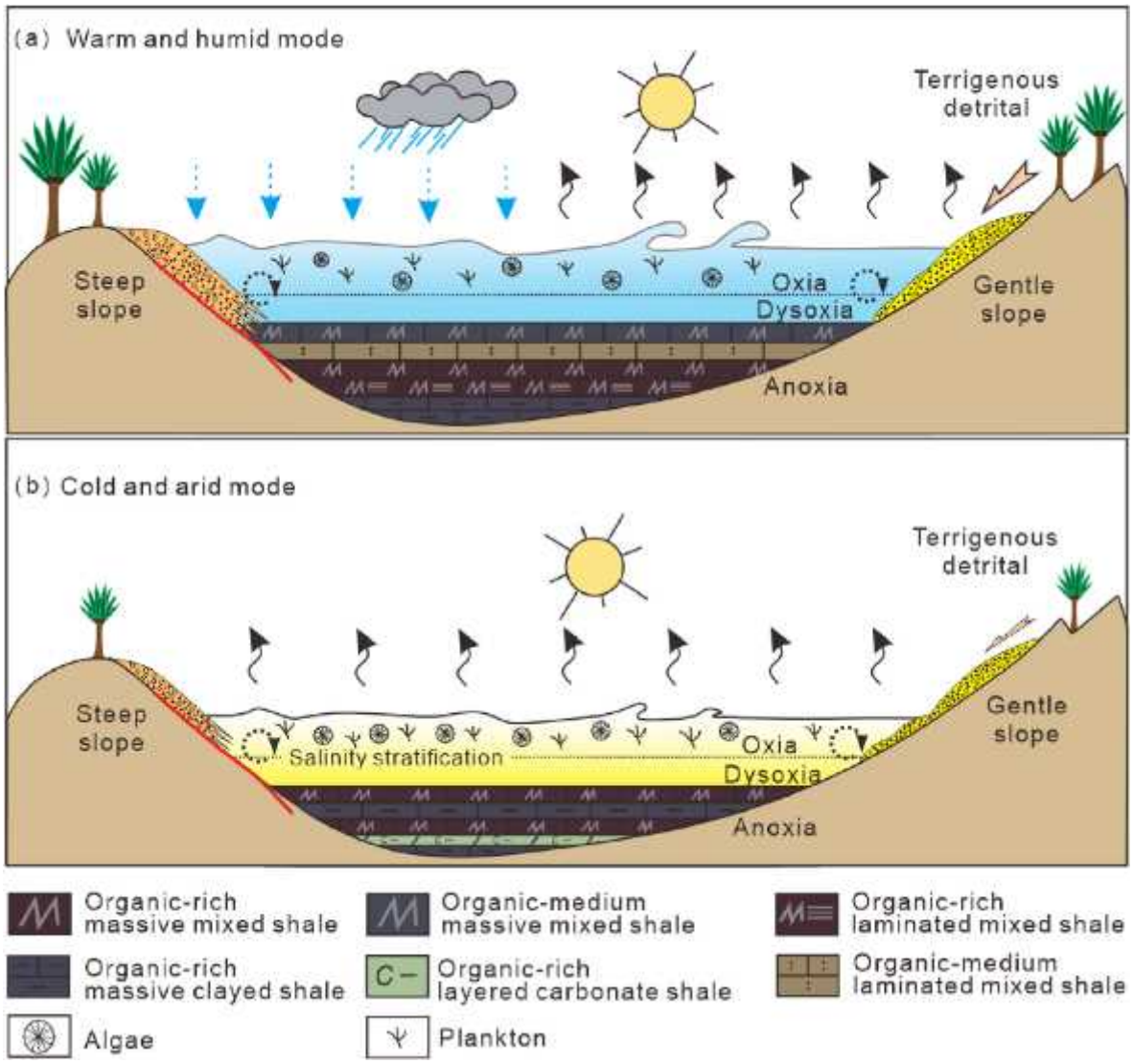

Fig. 18. A model of the development and distribution of the lithofacies in the lacustrine rift basin.

of terrigenous clastic materials. The rainfall is greater than the evaporation, resulting in low salinity water, which is not conducive to the precipitation of carbonate minerals and the formation of carbonate lamina. However, under dry and cold climate conditions in the provenance area, the ability of rivers to carry terrigenous debris is weakened due to weak weathering. The evaporation is greater than the precipitation, resulting in the high salinity water, and the carbonate minerals precipitate at the bottom of the lake to form a thin layer of carbonate rock.

On a microscope sedimentary scale, the seasonal alternation makes the vertical accretion of materials with different components (Zolitschka et al., 2015), and finally forms the micro lamina structure under the effect of burial depth compaction. The thickness of a single lamina is related to the deposition rate during the deposition period. This horizontal lamina is also mainly formed in relatively quiet stratified water bodies, and no cross-bedding, lenticular bedding and wavy bedding related to water transport are found (Gu et al., 2019; Li et al., 2020a, 2020b).

5.3. An sedimentary model of the lacustrine rift basin

Based on the above discussion, the sedimentary environment has significant control over lithofacies development in the study interval. The upper part of the study interval was deposited in warm and humid climate conditions, with abundant precipitation and high detrital supply, and the lake is deep in water and low in salinity. The shallow lake in the gentle slope zone was affected by terrigenous input and hydrodynamic conditions. Sandstone and siltstone with larger grain sizes are deposited here, mainly in massive structures, accompanied by a small amount of cross-bedding. At the same time, the content of terrigenous clastic minerals in fine-grained sediments is high, but organic matter is not easy to deposit and preserve, so the abundance of organic matter in rocks is low. The semi-deep lake was less affected by hydrodynamics. The fine-grained sediments from the source area settle down in this area, and the flocculation sedimentation of organic matter and clay minerals increased the content of organic matter, and the terrigenous clastic minerals and organic matter alternate to form a laminar structure. The water above CCD in the deep lake area is quiet. In addition to the flocculation and sedimentation of clay minerals and organic matter, carbonate minerals are precipitated (Jiang et al., 2013). Here we only try to understand the carbonate deposition process in the lacustrine rift basin by the concept of "carbonate compensation depth" of the ocean, that is, the precipitation of carbonate depends on the relationship between the production rate of carbonate and the dissolution rate, which is controlled by the depth of the water. Under the condition of water stratification, it is easy to form a flat lamina. However, carbonate below

CCD will no longer precipitate, and it is mainly supplied by very fine-grained terrigenous clay minerals, and the supply rate is slow, mainly by the flocculation of clay minerals and organic matter. Water stratification, blocking, and anoxic conditions are conducive to the preservation of organic matter, to form organic-rich laminated clayey shale. While the steep slope zone is dominated by coarse-grained sediments. Affected by the slope, terrigenous clasts can extend to the semi-deep and the deep lake (Fig. 18a).

Under cold and arid climate conditions, strong evaporation makes the lake level drop, the salinity of the water body increases, and the supply of terrigenous debris is less. Shallow water condition is not conducive to the preservation of organic matter, and it is easy to form organic-poor massive felsic shale and mixed shale. In the semi-deep lake, due to the rich nutrients brought by the shallow lake area and the deep lake area, the water is clear and sunny, the organisms usually grow in seasonal bursts, the biochemical effect is strong, and the carbonate minerals are enriched (Liu et al., 2020a, 2020b), forming organic-rich laminated carbonate shale. The deep lake area is also dominated by the supply of very fine-grained terrigenous clay minerals, mainly organic-rich laminated clayey shale (Fig. 18b).

6. Conclusions

(1) Based on observations in cores, thin sections, scanning electron microscope, and TOC analysis, this study systematically analyzed petrological characteristics of lacustrine shales from the Es_3^4 sub-member in Nanpu Sag. Es_3^4 sub-member is divided into 15 types of lithofacies. The lower part is mainly organic-medium massive mixed shale, the middle part is organic-rich massive mixed shale, and the upper part is organic-rich laminated mixed shale.

(2) The upper part has the most humid and warm climate conditions, strongest weathering, brackish-fresh water, lowest paleo-productivity, and dominant oxic condition. The middle part has cold and arid climate conditions, weakest weathering, highest paleo-productivity, and anoxic conditions. The lower part has an evident fluctuation in paleoclimate, salinity, productivity, and redox condition.

(3) Paleo-productivity and redox conditions are the basic conditions for the enrichment and preservation of organic matter. In addition, proper salinity and material supply provide favorable conditions for the enrichment and preservation of organic matter. The paleo-climate and paleo-salinity were the most critical factors controlling the mineral composition and laminae development. The highest terrigenous material and extremely developed clay and felsic laminae during the upper part were probably driven by the humid and warm climate and relatively low salinity conditions, and the highest carbonate minerals and few carbonate laminae in the lower part were probably driven by the cold and arid climate and relatively high salinity conditions.

Credit author statement

Huan Liu: Conceptualization, Writing–original draft, Investigation, Formal analysis. Xiaoping Liu: Conceptualization, Supervision, Investigation, Validation, Funding acquisition, Project administration, Writing–review & editing. Guoyong Liu: Conceptualization, Resources. Guoyong Li: Methodology, Resources. Jianwei Wang: Methodology, Investigation. Yongliang Gao: Methodology, Data curation. Biao Sun: Methodology, Investigation. Jiakai Hou: Validation, Investigation. Hanxi Liu: Validation, Investigation. Xuejiao Sun: Investigation.

Declaration of competing interest

The authors declare that we have no known competing financial interests or personal relationships that could have appeared to influence the work reported in this paper.

Data availability

The data that has been used is confidential.

Acknowledgment

This work was financially supported by the National Natural Science Foundation of China (Grant No. 42072150). We acknowledge the Associate Editor, all anonymous reviewers, and professor Liu Bo in the Northeast Petroleum University for the valuable comments which significantly improved the revised manuscript. We are grateful to the PetroChina Jidong Oilfield for providing data access, and permission to publish.

References

Algeo, T.J., Li, C., 2020. Redox classification and calibration of redox thresholds in sedimentary systems. Geochem. Cosmochim. Acta 287 (3–4).
Algeo, T.J., Maynard, J.B., 2004. Trace-element behavior and redox facies in core shales of Upper Pennsylvanian Kansas-type cyclothems. Chem. Geol. 206 (3–4), 289–318.
Algeo, T.J., Tribovillard, N., 2009. Environmental analysis of Paleoceanographic systems based on Molybdenum–Uranium covariation. Chem. Geol. 268 (3), 211–225.
Anderson, R.Y., Dean, W.E., 1988. Lacustrine varve formation through time. Palaeogeogr. Palaeoclimatol. Palaeoecol. 62 (1–4), 215–235.
Aplin, A.C., Macquaker, J.H.S., 2011. Mudstone diversity: origin and implications for source, seal, and reservoir properties in petroleum systems. AAPG Bull. 95 (12), 2031–2059.
Chen, C., et al., 2016a. The geochemical characteristics and factors controlling the organic matter accumulation of the Late Ordovician-Early Silurian black shale in the Upper Yangtze Basin, South China. Mar. Petrol. Geol. 76, 159–175.
Chen, D., et al., 2021. Organic geochemical characteristics and shale oil potential of the middle Eocene early-mature shale in the Nanpu Sag, Bohai Bay Basin, Eastern China. Mar. Petrol. Geol. (4), 105248
Chen, S.B., et al., 2011. Characteristics and significance of mineral compositional of Lower Silurian Longmaxi Formation shale gas reservoir in the southern margin of Sichuan Basin. Acta Pet. Sin. 32 (5), 775–782 (in Chinese with English abstract).
Chen, S.Y., et al., 2016b. Lithofacies types and reservoirs of Paleogene fine-grained sedimentary rocks Dongying sag, Bohai Bay Basin, China. Petrol. Explor. Dev. Online 43 (2).
Clarkson, M.O., et al., 2014. Assessing the utility of Fe/Al and Fe-speciation to record water column redox conditions in carbonate-rich sediments. Chem. Geol. 382, 111–122.
Curran, K.J., et al., 2002. Fine-grained suspended sediment dynamics in the Eel River flood plume. Continent. Shelf Res. 22 (17).
Deer, W.A., et al., 1966. An Introduction to the Rock-Forming Mineral. Prentice Hall, pp. 1–712.
Eisma, D., 1986. Flocculation and de-flocculation of suspended matter in estuaries. Neth. J. Sea Res. 20 (2–3), 183–199.
Fedo, C.M., et al., 1995. Unraveling the effects of potassium metasomatism in sedimentary rocks and paleosols, with implications for paleoweathering conditions and provenance. Geology 23 (10), 921–924.
Feng, Z., 2019. A review on the definitions of terms of sedimentary facies. J. Palaeogeogr. (Engl. Ed. (4), 321–331.
Flügel, E., 2010. Microfacies of Carbonate Rocks: Analysis, Interpretation and Application. Berlin and Heidelberg GmbH & Co.
Francois, R., et al., 1995. Biogenic barium fluxes to the deep sea: implications for paleoproductivity reconstruction. Global Biogeochem. Cycles 9 (2), 289–303.
Griffith, E.M., Paytan, A., 2012. Barite in the ocean – occurrence, geochemistry, and palaeoceanographic applications. Sedimentology 59 (6), 1817–1835.
Gu, Y.T., et al., 2019. Characteristics of Fine-Grained Sedimentary Laminae of Shale in Niutitang Formation, Guizhou, the 17th Annual Meeting of China Society of Mineral and Rock Geochemistry. Abstracts Of The 17th Annual Meeting Of The Chinese Society of Mineral And Rock Geochemistry, Hangzhou, Zhejiang, China, pp. 1072–1073.
Håkanson, L. et al., Sediment trap assemblages - a methodological description. Hydrobiologia, 176–177(1): 481-490.
Hou, H., et al., 2022. Effect of paleoclimate and paleoenvironment on organic matter accumulation in lacustrine shale: constraints from lithofacies and element geochemistry in the northern Qaidam Basin, NW China. J. Petrol. Sci. Eng. 208, 109350.
Hou, J.K., et al., 2023. Effect of shale lithofacies on pore structure in the first member of Shahejie formation, Nanpu sag[J]. J. China Inst. Min. Technol. 52 (1), 91–105 (in Chinese with English abstract).
Jia, C.Z., et al., 2014. Four important theoretical issues of unconventional petroleum geology. Acta Pet. Sin. 35 (1), 1–10 (in Chinese with English abstract).
Jiang, Y., et al., 2020. Recognizing the internal structure of normal faults in clastic rocks and its impact on hydrocarbon migration: a case study from Nanpu Depression in the Bohai Bay Basin, China. J. Petrol. Sci. Eng. 184, 106492.
Jiang, Z., et al., 2017. Classification of hydrocarbon-bearing fine-grained sedimentary rocks. J. Earth Sci. 28 (6), 963–976.

Jiang, Z.X., et al., 2013. Several issues in sedimentological studies on hydrocarbon-bearing fine-grained sedimentary rocks. Acta Pet. Sin. 34 (6), 1031–1039 (in Chinese with English abstract).
Jin, Z., et al., 2021. Several issues worthy of attention in current lacustrine shale oil exploration and development. Petrol. Explor. Dev. 48 (6), 14.
Kassem, A.A., et al., 2022. Paleoenvironment, sequence stratigraphy and source rock potentiality of the Cenomanian-Turonian boundary sediments of Southern Tethys. Mar. Petrol. Geol. 139, 105624.
Krumbein, W.C., 1932. The mechanical analysis of fine-grained sediments. J. Sediment. Res. 2 (3), 140–149.
Latimer, J.C., Filippelli, G.M., 2002. Eocene to Miocene terrigenous inputs and export production: geochemical evidence from ODP Leg 177, Site 1090. Palaeogeogr. Palaeoclimatol. Palaeoecol. 182 (3–4), 151–164.
Li, B., et al., 2019a. Lithofacies and pore characterization in an argillaceous-siliceous-calcareous shale system: a case study of the Shahejie Formation in Nanpu sag, Bohai Bay Basin, China. J. Petrol. Sci. Eng. 173, 804–819.
Li, B., et al., 2019b. Lithofacies and pore characterization in an argillaceous-siliceous-calcareous shale system: a case study of the Shahejie Formation in Nanpu sag, Bohai Bay Basin, China. J. Petrol. Sci. Eng. 173.
Li, M., et al., 2022. Diversity in the lithofacies assemblages of marine and lacustrine shale strata and significance for unconventional petroleum exploration in China. Oil Gas Geol. 43 (1), 1–25 (in Chinese with English abstract).
Li, Q., et al., 2020a. Major and trace element geochemistry of the lacustrine organic-rich shales from the Upper Triassic Chang 7 Member in the southwestern Ordos Basin, China: implications for paleoenvironment and organic matter accumulation. Mar. Petrol. Geol. 111, 852–867.
Li, T., et al., 2015. Characteristics and Research Significance of Fine Lacustrine Sedimentary Rock Laminations of Xiagou Formation in Qingxi Depression of Jiuquan Basin. China Petroleum Exploration (in Chinese with English abstract).
Li, W., et al., 2020b. Characteristics and forming mechanism of laminae fine-grained sedimentary rock of the Paleogene funing Formation in Gaoyou and Jinhu sags, Subei basin. J. Palaeogeogr. 22 (3), 469–482.
Li, Y., et al., 2021. Paleoenvironment reconstruction of the upper Paleozoic in the Linxing area, northeastern Ordos basin, China. AAPG (Am. Assoc. Pet. Geol.) Bull. 12, 105.
Liang, C., et al., 2018. Sedimentary environmental controls on petrology and organic matter accumulation in the upper fourth member of the Shahejie Formation (Paleogene, Dongying depression, Bohai Bay Basin, China). Int. J. Coal Geol. 186, 1–13.
Liang, C., et al., 2022. Storage space development and hydrocarbon occurrence model controlled by lithofacies in the Eocene Jiyang Sub-basin, East China: significance for shale oil reservoir formation. J. Petrol. Sci. Eng. 215, 110631.
Liu, B., et al., 2018. Petrological characteristics and shale oil enrichment of lacustrine fine-grained sedimentary system: a case study of organic-rich shale in the first member of Cretaceous Qingshankou Formation in Gulong Sag, Songliao Basin, NE China. Petrol. Explor. Dev. 45 (5), 884–894.
Liu, B., et al., 2019. Lithofacies and depositional setting of a highly prospective lacustrine shale oil succession from the upper Cretaceous Qingshankou Formation in the Gulong sag, northern Songliao basin, Northeast China. AAPG (Am. Assoc. Pet. Geol.) Bull. 103, 405–432.
Liu, C.L., et al., 2001. Algal blooms: the primary mechanism in the formation of lacustrine petroleum source rocks. Geol. Rev. 2, 207–210+8 (in Chinese with English abstract).
Liu, H., et al., 2020a. Sedimentary environment and lithofacies of fine-grained hybrid sedimentary in Dongying sag: a case of fine-grained sedimentary system of the Es4. Earth Sci. 45 (10), 3543–3555.
Liu, Z., et al., 2020b. Lithofacies types and assemblage features of continental shale strata and their implications for shale gas exploration: a case study of the Middle and Lower Jurassic strata in the Sichuan Basin. Nat. Gas. Ind. B 7 (4), 358–369.
Lobza, J.S.V., 1999. Biogenic sedimentary structures produced by Worms in Soupy, Soft muds: observations from the Chattanooga shale (upper Devonian) and experiments. J. Sediment. Res. 69.
Loucks, R.G., et al., 2012. Spectrum of pore types and networks in mudrocks and a descriptive classification for matrix-related mudrock pores. AAPG Bull. 96 (6), 1071–1098.
Lu, S.F., et al., 2012. Classification and evaluation criteria of shale oil and gas resources: discussion and application. Petrol. Explor. Dev. 39 (2), 268–276.
Ma, B., et al., 2022. Geochemical characteristics and depositional paleoenvironment of source rocks from the lower Cretaceous Chijinbao Formation in Jiuxi basin, China. J. Petrol. Sci. Eng. 210, 109968.
Mclennan, S.M., 2001. Relationships between the trace element composition of sedimentary rocks and upper continental crust. G-cubed 2 (4).
Miall, A.D., Andrew, D., 1990. Principles of Sedimentary Basin Analysis. Springer Verlag, pp. 1–628.
Morford, J.L., 1999. The geochemistry of redox sensitive trace metals in sediments. Geochim. Cosmochim. Acta 63 (2), 1735–1750.
Negri, A., 1996. Possible origin of laminated sediments of the anoxic Bannock Basin (eastern Mediterranean). Geo Mar. Lett. 16 (2), 101–107.
Nelson, B.W., 1967. Sedimentary phosphate method for estimating paleosalinities. Science 158 (3803), 917–920.
Nesbitt, H.W., Young, G.M., 1984. Prediction of some weathering trends of plutonic and volcanic rocks based on thermodynamic and kinetic considerations. Geochem. Cosmochim. Acta 48 (7), 1523–1534.
Nesbitt, H.W., et al., 1996. Effects of chemical weathering and Sorting on the petrogenesis of Siliciclastic sediments, with implications for provenance studies. J. Geol. 104 (5), 525–542.
Pan, S.X.,et al, 2014. Deepwater bottom current rework Sand(BCRS) in lacustrine basins: sedimentary characteristics, identification criterion, formation mechanism and its significance for unconventional oil/gas exploration. Nat. Gas Geosci., 2014, 25(10): 1577-1585.
Panahi, A., et al., 2000. Behavior of major and trace elements (including REE) during Paleoproterozoic pedogenesis and diagenetic alteration of an Archean granite near Ville Marie, Québec, Canada. Geochem. Cosmochim. Acta 64 (13), 2199–2220.
Paytan, A., Griffith, E.M., 2007. Marine barite: recorder of variations in ocean export productivity. Deep-Sea Res. Part II 54 (5–7), 687–705.
Picard, M.D., 1971. Classification of fine-grained sedimentary rocks. J. Sediment. Res. 41 (1).
Piper, D.Z., Calvert, S.E., 2009. A marine biogeochemical perspective on black shale deposition. Earth Sci. Rev. 95 (1–2), 63–96.
Potter, P.E., et al., 2005. Mud and Mudstones: Introduction and Overview. Springer, Berlin, pp. 1–297.
Qiu, Z., et al., 2021. Accumulation of sediments with extraordinary high organic matter content: insight gained through geochemical characterization of indicative elements. Oil Gas Geol. 42 (4), 931–948 (in Chinese with English abstract).
Qiu, Z., Zou, C.N., 2020. Unconventional petroleum Sedimentology: Connotation and prospect. Acta Sedimentol. Sin. 38 (1), 1–29 (in Chinese with English abstract).
Radwan, A.E., et al., 2022. Chapter Twelve - gas adsorption and reserve estimation for conventional and unconventional gas resources. In: Wood, D.A., Cai, J., Wood, D.A., Cai, J., Wood, D.A., Cais, J. (Eds.), *Sustainable Geoscience for Natural Gas Subsurface Systems. Gulf Professional Publishing, pp. 345–382.
Raiswell, R., De Canfield, 1998. Sources of iron for pyrite formation in marine sediments. Am. J. Sci. 298 (3), 219, 219.
Ran, B., et al., 2016. Lithofacies classification of shales of the lower Paleozoic Wufeng-Longmaxi formations in the Sichuan Basin and its surrounding areas, China. Earth Sci. Front. 22 (2), 96–107 (in Chinese with English abstract).
Rimmer, S.M., 2004. Geochemical paleoredox indicators in Devonian–Mississippian black shales, Central Appalachian basin (USA). Chem. Geol. 206 (3–4), 373–391.
Schieber, J., et al., 2007. Accretion of mudstone beds from migrating floccule ripples. Science 318 (5857), 1760–1763.
Schieber, J., et al., 2013. Experimental deposition of carbonate mud from moving suspensions: importance of flocculation and implications for modern and ancient carbonate mud deposition. J. Sediment. Res. 83 (11), 1026–1032.
Shinn, E.A., et al., 1993. Lime-mud layers in high-energy tidal channels: a record of hurricane deposition. Geology 21 (7), 603–606.
Shi, J., et al., 2020. Depositional process and astronomical forcing model of lacustrine fine-grained sedimentary rocks: a case study of the early Paleogene in the Dongying Sag, Bohai Bay Basin. Mar. Petrol. Geol. 113.
Taylor, S.R., Mclennan, S.M., 1985. The continental crust: its composition and evolution. J. Geol. 94 (4), 57–72.
Timothy, 2006. A critical look at iron paleoredox proxies: new insights from modern euxinic marine basins. Geochem. Cosmochim. Acta 70, 5698–5722.
Tribovillard, N., et al., 2006a. Trace metals as paleoredox and paleoproductivity proxies: an update. Chem. Geol. 232 (1–2), 12–32.
Tribovillard, N., et al., 2006b. Trace metals as paleoredox and paleoproductivity proxies: an update. Chem. Geol. 232 (1–2), 12–32.
Tripsanas, E.K., et al., 2007. Submarine mass-transport facies: new perspectives on flow processes from cores on the eastern North American margin. Sedimentology. 55 (1), 97–136.
Tyrrell, T., 1999. The relative influences of nitrogen and phosphorus on oceanic primary production. Nature 400 (6744), 525–531.
Walker, D., K, O.J.A., 1999. The characteristics and source of laminated mud at Lake Barrine, Northeast Australia. Quat. Sci. Rev. 18 (14), 1597–1624.
Wang, E., et al., 2022. Exploration potential of different lithofacies of deep marine shale gas systems: insight into organic matter accumulation and pore formation mechanisms. J. Nat. Gas Sci. Eng. 102, 104563.
Wang, G.M., Zhong, J.H., 2004. A review and the prospects of the researches on sedimentary mechanism of lacustrine laminae. Acta Petrol. Mineral. 23 (1), 43–48 (in Chinese with English abstract).
Wang, Y., et al., 2012. Reservoir characteristics of shale gas in Longmaxi formation of the lower Silurian, southern Sichuan. Shiyou Xuebao/Acta Petrol Sinica 33 (4), 551–561.
Wei, W., Algeo, T.J., 2019. Elemental proxies for paleosalinity analysis of ancient shales and mudrocks. Geochem. Cosmochim. Acta. 287, 341–366.
Williams, T.S., et al., 2022. Petrophysical analysis and mudstone lithofacies classification of the HRZ shale, North Slope, Alaska. J. Petrol. Sci. Eng. 208, 109454.
Wu, Z., et al., 2021. Sedimentary environment and organic enrichment mechanisms of lacustrine shale: a case study of the Paleogene Shahejie Formation, Qikou sag, Bohai Bay Basin. Paleogeogr. Palaeoclimatol. Palaeoecol. 573, 110404.
Yawar, Z., Schieber, J., 2017. On the origin of silt laminae in laminated shales. Sediment. Geol. 22–34.
Yuan, X.J., et al., 2015. Lacustrine fine-grained sedimentary features and organic-rich shale distribution pattern: a case study of Chang 7 Member of Triassic Yanchang Formation in Ordos Basin, NW China. Petrol. Explor. Dev. 42 (1), 37–47.
Zhang, M., Li, Z., 2018. The lithofacies and reservoir characteristics of the fine-grained sedimentary rocks of the Permian Lucaogou Formation at the northern foot of Bogda Mountains, Junggar Basin (NW China). J. Petrol. Sci. Eng. 170, 21–39.
Zhang, S., et al., 2017. Classification scheme for lithofacies of fine-grained sedimentary rocks in faulted basins of eastern China: insights from the fine-grained sedimentary rocks in Paleogene, southern Bohai Bay Basin. Acta Geol. Sin. 91 (5), 1108–1119 (in Chinese with English abstract).

Zhao, W.Z., et al., 2020. Accumulation contribution differences between lacustrine organic-rich shales and mudstones and their significance in shale oil evaluation. Petrol. Explor. Dev. (6), 12.
Zheng, H.J., et al., 2007. High-quality source rocks in Nanpu sag. Petrol. Explor. Dev. 34 (4), 385–391.
Zhou, L.H., et al., 2016. Several issues in studies on fine-grained sedimentary rocks. Lithol. Reservoirs 28 (1), 6–15 (in Chinese with English abstract).
Zolitschka, B., Francus, P., Ojala, A.E.K., Schimmelmann, A., 2015. Varves in lake sediments – a review. Quat. Sci. Rev. 117, 1–41.
Zou, C.N., et al., 2020. Shale oil and gas revolution and its impact. Acta Pet. Sin. 41 (1), 1–12 (in Chinese with English abstract).
Zou, C.N., et al., 2023. Formation and distribution potential of global shale oil and the theoretical and technological progress of continental shale oil in China[J/OL]. Earth Sci. Front. 30 (1), 128–142 (in Chinese with English abstract).